Identification of STK25 as a direct activator of LATS signaling

Sanghee Lim[1], Tenny Mudianto[1, 3], Hatim M. Mustaly [1], Ian Paolo Morelos Mauricio [1], Marc A. Vittoria [1], Ryan J. Quinton[1], Brian W. Howell [4], Hauke Cornils[5], Neil J. Ganem [1,2*].

[1]The Laboratory of Cancer Cell Biology, Department of Pharmacology and Experimental Therapeutics, Boston University School of Medicine, Boston, MA.
[2]Division of Hematology and Oncology, Department of Medicine, Boston University School of Medicine, Boston, MA.
[3]Department of Medical Oncology, Dana-Farber Cancer Institute, Harvard Medical School, Boston, MA.
[4]Department of Neuroscience and Physiology, SUNY Upstate Medical University, Syracuse, NY.
[5]Evotec, Hamburg, Germany.

*Correspondence to: Neil J. Ganem, e-mail: nganem@bu.edu

Neil J. Ganem
The Cancer Center
Boston University School of Medicine
72 E. Concord St. K-712C
Boston, MA 02118
Phone: (617) 638-5382

Keywords: tetraploid, tumor suppressor, TAZ, Hippo, WARTS, SOK1, YSK1

Abstract

LATS kinases integrate numerous cellular cues to restrict the oncoproteins YAP/TAZ in a phosphorylation-dependent fashion as part of the Hippo tumor suppressor pathway, yet upstream activators of LATS kinases remain incompletely characterized. We performed a focused RNAi-based kinome screen and identified the kinase STK25 as a previously uncharacterized activator of LATS. We demonstrate that loss of STK25 blunts the ability of cells to activate Hippo signaling and is sufficient to significantly increase levels of active YAP/TAZ to enhance cellular proliferation. In contrast to all known kinase activators of LATS, which phosphorylate the hydrophobic motif of LATS kinases to stimulate auto-phosphorylation, STK25 directly phosphorylates the activation loop motif of LATS. Interestingly, *STK25* is significantly focally deleted across a wide spectrum of human cancers, suggesting *STK25* loss may represent a major mechanism by which tumors are able to functionally impair the Hippo tumor suppressor pathway.

First discovered in *Drosophila* as a critical regulator of organ size, the Hippo tumor suppressor pathway has emerged as playing a major role in maintaining tissue homeostasis through regulation of cell proliferation. Key mediators of Hippo signaling are LATS1 and LATS2 (Large Tumor Suppressor) kinases, which function to negatively regulate the activity of the oncogenic transcriptional co-activators Yes-associated protein (YAP) and transcriptional co-activator with PDZ-binding motif (TAZ) (Zhang et al. 2009, Zhao et al. 2010). Upon stimulation of Hippo signaling, activated LATS kinases directly phosphorylate YAP/TAZ, which promotes their nuclear extrusion and subsequent degradation (Zhao et al. 2010). By contrast, in the absence of LATS activation, YAP/TAZ are free to translocate into the nucleus, where they bind to the TEAD/TEF family of transcription factors to promote the expression of numerous genes essential for cellular proliferation and survival (Wu et al. 2008, Zhang et al. 2008, Hong et al. 2005). Deregulation of LATS1/2 kinases, which leads to subsequent hyper-activation of YAP/TAZ, is sufficient to promote tumorigenesis in mouse models (Zhou et al. 2009, Nishio et al. 2015). Furthermore, amplification of YAP and/or TAZ has been found in a variety of human malignancies (Overholtzer et al. 2006, Fernandez-L et al. 2009).

Multiple signals lead to the activation of LATS kinases, including contact inhibition, cellular detachment, loss of actin cytoskeletal tension, serum deprivation, glucose starvation, signaling from G-protein coupled receptors, and cytokinesis failure (Zhao et al. 2010, Dupont et al. 2009, Adler et al. 2013, Mo et al. 2015, Wang et al. 2015, Ganem et al. 2014, Yu et al. 2012, Dutta et al. 2018). Mechanistically, LATS kinases were initially found to be regulated by MST1 and MST2 kinases, the mammalian orthologs of the Drosophila Hpo kinase, after which the pathway is named. Activation of LATS1/2 initiates with the recruitment of MST1/2 to LATS kinases via interactions

with scaffolding proteins such as SAV1, MOB1, and NF2 at the plasma membrane (Zhang et al. 2010, Yin et al. 2012). Once recruited, MST1/2 phosphorylate LATS1/2 at their hydrophobic motifs to remove the auto-inhibitory conformations of LATS1/2, thereby allowing auto- and trans-phosphorylation interactions to take place at the activation loop motifs of LATS1/2, subsequently leading to full LATS kinase activity. However, it has become increasingly clear that kinases that regulate the activation of LATS are not limited to MST1/2 in mammalian cells. Genetic deletion of MST1/2 fails to prevent full LATS activation, and YAP/TAZ phosphorylation remains intact in mice lacking MST1/2 (Zhou et al. 2009, Meng et al. 2015). Moreover, several conditions known to stimulate LATS activation, such as contact inhibition, serum starvation, and cell detachment, do so in a MST1/2-independent manner, suggesting evolutionary divergence from *Drosophila* in mammalian cells, as well as the presence of additional upstream kinases that control LATS activation (Ganem et al. 2014, Zhou et al. 2009, Dutta et al. 2018, Plouffe et al. 2016). Indeed, recent work has shown the presence of additional upstream kinases that control LATS activation outside of MST1/2, as several members of the MAP4K family have been identified as having redundant roles in directly phosphorylating the hydrophobic motif of LATS kinases (Zheng et al. 2015, Meng et al. 2015). However, cells in which *MST1/2* and all *MAP4K*s have been collectively deleted with CRISPR-mediated approaches still induce LATS and YAP phosphorylation upon stimulation, albeit at significantly reduced levels, indicating that other upstream activators of LATS kinases exist (Meng et al. 2015, Plouffe et al. 2016). Given that Hippo pathway inactivation has been found across numerous tumor types, but mutations and deletions of core Hippo signaling components are rare, the identification of novel upstream activators of Hippo signaling carries the potential to uncover previously unappreciated tumor suppressor genes (Pan D 2010, Kelliher and O'Sullivan 2013).

To identify novel upstream kinases that regulate LATS activity, we performed a focused RNAi screen to identify kinases that contribute to LATS phosphorylation and subsequent YAP phosphorylation. This approach identified STK25 as a novel upstream activator of the LATS kinases, whose loss significantly promotes YAP/TAZ activity. Mechanistically, we demonstrate that STK25 phosphorylates LATS at the activation loop motif in the absence of hydrophobic motif phosphorylation, which distinguishes it from all of the other known LATS activating kinases discovered to date.

Results

A focused kinome screen identifies STK25 as a novel regulator of LATS-YAP phosphorylation

We performed a focused RNAi screen to identify kinases that are necessary for inducing YAP phosphorylation under conditions of activated Hippo signaling in the non-transformed IMR90 fibroblast cell line. We focused our kinome screen on members of the Sterile20 superfamily of kinases (which includes MST1/2), as members of this superfamily maintain structural similarities in spite of evolutionary divergence (Thompson and Sahai 2014). We depleted individual kinases via RNAi and then stimulated Hippo pathway activation by treatment with the drug dihydrocytochalasin B (DCB), which destabilizes the actin cytoskeleton and mimics activation of Hippo signaling under loss of F-actin driven cytoskeletal tension (MacLean-Fletcher and Pollard 1980, Zhao et al. 2012). Treatment with DCB induced robust activation of Hippo signaling with consequent phosphorylation of YAP at serine 127, which is a LATS-specific canonical site that regulates YAP cytoplasmic retention through binding to 14-3-3 proteins (Zhao et al. 2010). As expected, we found that depletion of known activators of LATS, such as MST1/2, decreased YAP

phosphorylation, but surprisingly we found STK25 to be the strongest hit in our screen (Figure S1A-D). Depletion of STK25 significantly reduced levels of YAP S127 phosphorylation as assessed by quantitative immunoblotting relative to controls in this assay (Figures S1A-D). Importantly, this effect was reproduced in multiple cell lines, including both HEK293A and hTERT RPE-1 (Figure 1A, S1C-D). We performed phos-tag gel electrophoresis to assess overall levels of YAP phosphorylation and found that STK25-depletion led to significantly reduced levels of phosphorylated YAP, with consequent enrichment of unphosphorylated YAP, as compared to controls (Figure 1B). Additionally, we found that TAZ, a mammalian paralog of YAP, was also enriched in an unphosphorylated status in STK25-depleted cells (Figure 1C). We reproduced these results in cells treated with Latrunculin A, which is a fungal-derived actin-binding toxin that has a different mechanism of action than cytochalasin-class agents (Fig S1E) (Morton et al. 2000).

We used multiple approaches to ensure that decreases in YAP phosphorylation following STK25 depletion via RNAi was not due to RNAi-induced off-target effects. First, we validated this finding with multiple distinct siRNA sequences targeting STK25 (8 total siRNAs, including three targeting the 3'UTR), and we observed that the degree of reduction in YAP phosphorylation strongly correlated with STK25 knockdown efficiency (Figure S1F-G). Second, we used CRISPR-Cas9 to genetically knockout STK25 from HEK293A cells and found that STK25 KO clonal cells (generated with two different sgRNA sequences) similarly failed to induce YAP phosphorylation to the same extent as control cells expressing Cas9 and a non-targeting sgRNA following DCB treatment (Figure 1D). Finally, we demonstrated that overexpression of siRNA-resistant wild-type STK25, but not kinase-dead STK25 ^{K49R}, was sufficient to rescue the loss of YAP phosphorylation

observed in our knockdown experiments (Figures 1E). Altogether, these data reveal that the kinase STK25 plays a previously unappreciated role in promoting YAP phosphorylation.

STK25 Depletion Promotes YAP Activation

We next analyzed if the decrease in YAP phosphorylation following STK25 depletion leads to a corresponding increase in the nuclear localization of active YAP. Depletion of STK25, either by RNAi-mediated knockdown or CRISPR-mediated gene knockout, led to a significant increase in nuclear YAP in multiple cell lines (Figures 2A-F, S2D-I). We also observed a gene dose-dependent increase in nuclear YAP in *STK25*$^{-/-}$ and *STK25*$^{+/-}$ MEFs (Figures S2A-C). Remarkably, we found that depletion of STK25 enabled a population of YAP to remain nuclear even under conditions of actin depolymerization, which strongly sequesters YAP in the cytoplasm in control cells (Figure 2A-C).

To confirm that nuclear localized YAP was active, we first assessed whether depletion of STK25 increased YAP/TAZ activity using a luciferase-based gene expression reporter assay. HEK293A cells were transfected with a reporter encoding a YAP/TAZ-responsive luciferase gene, in which eight TEAD-YAP binding sites are cloned into the promoter driving expression of firefly luciferase (Dupont et al. 2011). Using this approach, we found that depletion of STK25 resulted in a doubling of expression from the luciferase reporter, indicating that loss of STK25 promotes YAP/TAZ activity (Figure 2I). We also assessed the expression of YAP-target genes in cells depleted of STK25 and found that canonical YAP-target genes were significantly upregulated in IMR90 fibroblasts (Figure 2G). Moreover, we found that YAP-target gene expression was also increased in a STK25 gene-dose dependent fashion in knockout MEFs for three well-established genes

(Figure 2H). Lastly, to assess gene expression in a comprehensive, unbiased fashion, we depleted STK25 from hTERT-RPE-1 cells and performed gene expression microarray analysis to obtain a list of genes that were significantly upregulated in cells lacking STK25 compared to controls. Gene Set Enrichment Analysis (GSEA) was performed using a curated set of 11 publically available, published gene sets for active YAP/TAZ as well as a composite gene set derived from RPE-1 cells expressing constitutively active YAP ^{S5A} or TAZ ^{4SA}. This GSEA revealed that depletion of STK25 in RPE-1 cells results in a highly significant enrichment of active YAP/TAZ gene expression signatures (Figures 2J, Figure S3A-B). Collectively, our data demonstrate that loss of STK25 promotes YAP/TAZ activation.

STK25 acts through LATS1/2 to inhibit YAP

Given that loss of STK25 leads to an overall decrease in phosphorylation of YAP, we predicted that overexpression of STK25 may have the opposite effect and promote phosphorylation of YAP. Indeed, we found that overexpression of wild-type STK25, but not a kinase dead mutant (STK25 ^{K49R}) led to significant increases in levels of phosphorylated YAP relative to controls (Figures 3A-B) and that this caused YAP to become enriched in the cytoplasm (Figure 3C-E). We found that this effect of STK25 on YAP phosphorylation was LATS1/2-dependent, as overexpression of STK25 in HEK293A cells genetically depleted of LATS1/2 by CRISPR (LATS1/2 dKO) did not produce cytoplasmic enrichment of YAP (Figures 4B-D). We also depleted STK25 from both wild-type and LATS dKO 293A cells and found that while loss of STK25 reduces YAP phosphorylation and drives YAP into the nucleus in wild-type cells, there was no such effect in LATS dKO 293A (Figures 4E-H), further indicating that STK25 functions through LATS1/2. Lastly, we found that knockdown of LATS1/2 via RNAi was sufficient to rescue YAP-target gene

expression, even upon STK25 overexpression (Figure 4A). Thus, STK25 depends on LATS1/2 to regulate YAP.

Interestingly, this STK25-LATS1/2 axis is independent of other identified upstream LATS-activating kinases. HEK293A cells depleted of MST1, MST2, and all members of the MAP4K family (MAP4K1-7) via CRISPR-Cas9 (henceforth called MM8KO 293A) still demonstrate YAP phosphorylation when grown to confluence, albeit at much lower levels than in wild-type 293A. However, MM8KO 293A cells depleted of STK25 showed significantly decreased levels of YAP phosphorylation (Figures S4A). Additionally, overexpression of STK25 in MM8KO 293A was sufficient to induce a cytoplasmic shift of YAP (Figures S4B-C). This suggests that STK25 acts to regulate YAP in a LATS1/2-dependent fashion and that this signaling is independent of MST1/2/MAP4Ks' activities.

STK25 stimulates LATS kinases by promoting phosphorylation of LATS on the activation loop motif

Since STK25 is sufficient to induce YAP phosphorylation in the absence of other upstream LATS-activating kinases, and given the structural similarities between STK25 and MST1/2, we tested if STK25 directly phosphorylates and activates LATS. We first assessed whether STK25 and LATS interact. We expressed HA-tagged LATS2 and FLAG-tagged STK25 in HEK293A cells and found that immunoprecipitated HA-tagged LATS2 co-precipitated FLAG-tagged STK25 (Figure 5A). To assess whether LATS1 or LATS2 bind to endogenous STK25, we overexpressed either Myc-tagged LATS1 or HA-tagged LATS2, and then immunoprecipitated each respective LATS kinase.

We found that endogenous STK25 co-precipitated with both LATS1 and LATS2, suggesting that STK25 interacts with both LATS kinases to promote their activation (Figure 5B).

We next tested if STK25 could directly phosphorylate LATS. To do this, we carried out an *in vitro* kinase assay using HA-LATS2 as the substrate and either FLAG-STK25 or FLAG-MAP4K1 (positive control) as the kinase after proteins were immunoprecipitation-purified from transfected HEK293A lysates (Figure 5C). As expected, we found that FLAG-MAP4K1 induced phosphorylation at the hydrophobic motif of LATS (LATS-HM), leading to subsequent phosphorylation at the activation loop (LATS-AL) (Figure 5D). By contrast, STK25 did not induce phosphorylation at the LATS-HM, but was able to induce phosphorylation at the LATS-AL (Figure 5D). This effect was dependent on STK25 kinase activity, as a kinase-dead STK25^{K49R} was unable to produce robust phosphorylation at the LATS-AL (Figure 5D). Altogether, these data suggested that STK25 might be acting to activate LATS through direct phosphorylation at the activation loop site, bypassing phosphorylation at the hydrophobic motif.

To verify that STK25, and not other identified upstream activators of LATS kinases such as MST1/2 and members of the MAP4K family were responsible for the increase in phosphorylation at the activation loop of LATS, we utilized MM8KO 293A cells to IP purify STK25 and LATS2 for our *in vitro* kinase reactions as before. Once again, co-incubation of wild-type FLAG-STK25 with HA-LATS2 produced robust increases in phosphorylation at the activation loop of LATS2 as assessed by immunoblotting, which was decreased when LATS2 was co-incubated with kinase-dead STK25 ^{K49R} (Figure S5A). As phosphorylation at the activation loop has been canonically associated with LATS auto-phosphorylation, we wished to further verify that STK25 kinase

activity, and not LATS2 intrinsic kinase activity, was driving this phenomenon (Tamaskovic et al. 2002, Stegert et al. 2004, Ni et al. 2015, Hoa et al. 2016). To accomplish this, we utilized LATS dKO 293A cells, into which kinase-dead LATS2 ^{D809A} was transfected. FLAG-STK25 and FLAG-MAP4K1 were also transfected into LATS dKO 293A cells. These proteins were IP-purified as before from the LATS dKO 293A cell lysates, which were then used for downstream *in vitro* kinase assays. Such a set-up ensured that we would be utilizing only LATS2 with no intrinsic kinase activity as our substrate, and that there would be no wild-type LATS1 or LATS2 that co-immunoprecipitated with either HA-LATS2 ^{D809A}, FLAG-STK25, or FLAG-MAP4K1 to confound interpretation of the data. Our results revealed that wild-type STK25, but not kinase-dead STK25 ^{K49R}, promoted the phosphorylation of LATS-AL, independent of LATS intrinsic kinase activity (Figure 5E). Further, we also noted that while MAP4K1 was able to promote phosphorylation of kinase-dead LATS2 at the hydrophobic motif, it was unable to do so at the activation loop. These data reveal that STK25 activates LATS kinases through a mechanism that is completely distinct from what has previously been characterized for the MST/MAP4K kinases (Figure 5E).

To assess whether the increase in phosphorylated LATS-AL correlates with an increase in LATS activity, we transfected STK25 either alone, or together with LATS2, in LATS dKO 293A cells and then assessed levels of YAP phosphorylation via immunoblotting. As we previously noted, overexpression of STK25 in LATS dKO 293A was insufficient to induce YAP phosphorylation; however, transfection of wild-type LATS2 was sufficient to increase levels of phosphorylated YAP, which was further increased upon co-transfection of LATS2 with STK25 ^{WT}, but not STK25 ^{K49R} (Figure S5B). Additionally, transfection of kinase-dead LATS2 abrogated this effect, which

could not be rescued by co-transfection with STK25, strongly indicating once again that STK25 depends upon LATS kinases for its inhibitory effects on YAP (Figure S5B).

To further validate our *in vitro* findings that STK25 is able to phosphorylate LATS at its activation loop, we assessed the effects that modulation of STK25 has on LATS-AL phosphorylation in cells. To do this, we depleted STK25 via siRNA transfection and then stimulated LATS activity by treating cells with 10 µM DCB, after which the levels of activated LATS were assessed by quantitative immunoblotting. We observed an increase in phosphorylated LATS-AL with DCB treatment, which was significantly decreased upon knockdown of STK25 (Figure 5F). Next, we overexpressed STK25 together with LATS2 in cells and found that co-expression of LATS2 along with wild-type STK25, but not kinase-dead STK25, was able to increase levels of phosphorylated LATS-AL (Figures 5G). Lastly, we grew to confluence either control HEK293A cells expressing Cas9 together with a non-targeting sgRNA or STK25 KO HEK293A expressing Cas9 together with a sgRNA targeting STK25, and then assessed levels of phosphorylated LATS1 at the hydrophobic motif (LATS-HM) and the activation loop (LATS-AL) by quantitative immunoblotting. We found a significant decrease in phosphorylation of the LATS-AL in our STK25 KO HEK293A, but to our surprise, we also noted a robust and seemingly compensatory increase in phosphorylation of the LATS-HM (Figure 5H). Further, this data suggested that cells lacking STK25 are unable to appropriately phosphorylate LATS-AL even when the LATS-HM is phosphorylated (Figure 5H). Taken together, these data demonstrate that STK25 activates LATS through a previously unreported mechanism in which STK25 directly promotes phosphorylation of LATS-AL, independent from LATS intrinsic kinase activity.

STK25 Loss Impairs LATS Activation upon Contact Inhibition and Cell Detachment and Provides a Proliferative Advantage

We next analyzed the effects of STK25 in physiologically relevant contexts that are known to stimulate LATS activation. We first assessed both LATS and YAP activity in confluent, contact inhibited cells, as contact inhibited cells are known to have strong activation of LATS kinases (Zhao et al. 2012). Indeed, we found that control HEK293A cells efficiently activated LATS and induced YAP phosphorylation upon being grown to full confluence (Figure 6A, S6A). By contrast, HEK293A cells depleted of STK25 exhibited reduced levels of YAP phosphorylation as assessed by quantitative immunoblotting (Figure 6A) and phos-tag analysis (Figure S6B). We also observed reduced TAZ phosphorylation and subsequent stabilization of unphosphorylated TAZ levels following loss of STK25 (Figures S6C). These results were reproduced in STK25 KO 293A cells (Figure S6D). We also grew adherent cells in suspension for defined periods of time, as cell detachment is another known activator of LATS activity (Zhao et al. 2012). We found that depletion of STK25 significantly impairs the dynamics of YAP phosphorylation under these conditions, such that not only does the overall magnitude of YAP phosphorylation become blunted, but YAP gets phosphorylated more slowly and to a lesser extent in STK25-depleted cells compared to controls (Figure 6D). Together, these results demonstrate that STK25 plays a significant role in activating LATS kinases following cellular perturbations known to activate the Hippo signaling pathway.

We hypothesized that depletion of STK25, with subsequent YAP activation, would also provide proliferative advantages to cells. Indeed, we found that cells genetically depleted of STK25 have an increased growth rate in culture (Figure 6B). We also found that depletion of STK25 allows

cells to partially overcome cell cycle arrest induced by contact inhibition, thereby validating our findings that loss of STK25 prevents YAP phosphorylation under contact inhibited conditions (Figure 6C). Further, it has previously been demonstrated that tetraploid cells, which arise from cytokinetic failures, fail to proliferate efficiently due to LATS activation and subsequent inactivation of YAP. Proliferation can be restored to tetraploid cells through restoration of YAP activity (Ganem et al. 2014). Indeed, we found that STK25 knockdown is also sufficient to restore proliferative capacity to tetraploid cells (Figures 6E-F).

Our data suggest STK25 is a novel activator of the LATS kinases whose depletion leads to activation of YAP/TAZ and subsequent cellular proliferation. YAP/TAZ are known to be hyper-activated across a wide range of human malignancies, although the mechanisms leading to their activation remain poorly understood. Our data suggest that loss of STK25 may represent one route through which cancer cells functionally activate YAP/TAZ. Interestingly, bioinformatic analysis of the TCGA reveals that focal deletion of *STK25* is a very common event across many tumor subtypes, with deep deletions occurring in a significant proportion of multiple aggressive cancers (Figure 7A). For example, *STK25* is homozygously deleted from nearly 9% of all sarcomas. We assessed if *STK25* deletion status has an effect on the clinical course of disease and found that sarcoma patients with *STK25* deletions have significantly shorter durations of survival than those with intact *STK25* and that deletions of *STK25* are more common in patients with recurrent disease than those without (Figures 7B and S7A). Additionally, we found that this pattern of recurrent focal loss in human cancers is unique to *STK25* among the currently identified LATS activating kinases (Figure S7B). Taken together, our findings suggest that loss of *STK25* may be one

mechanism through which human cancers functionally inactivate Hippo signaling to promote tumorigenesis and disease progression.

Discussion

It has been well established since the first knockout studies that deletions of both *MST1* and *MST2* are not sufficient to completely inactivate LATS signaling in mammalian cells (Zhou et al. 2009), strongly indicating the presence of additional LATS regulators (Thompson and Sahai 2015). Indeed, members of the MAP4K family, including human orthologs of *Drosophila* Hppy (MAP4K1, 2, 3, and 5) and Msn (MAP4K4, 6, and 7) were recently identified as upstream activators of LATS kinases. Like MST1/2, MAP4K proteins activate LATS via phosphorylation of the LATS hydrophobic motif (Li et al. 2014, Zheng et al. 2015, Meng et al. 2015, Hoa et al. 2016). The presence of such redundancies highlights the critical nature of LATS signaling in ensuring that cellular proliferation ceases when appropriate. In contrast, STK25-dependent activation of LATS entirely bypasses the need for phosphorylation at the hydrophobic motif, which provides some explanation for the robustness with which loss of this singular kinase is able to blunt LATS activation. Further, our study has revealed that LATS phosphorylation at the activation loop is not solely an auto- or trans-phosphorylation event, as we have identified STK25 as the first kinase able to phosphorylate the LATS activation loop motif independent of LATS kinase activity. It has previously been shown by several groups that while genetic deletion of the MST/MAP4K pathway components potently decreases levels of LATS and YAP phosphorylation, it is still possible to induce additional LATS activity upon treatment with actin depolymerizing agents or contact inhibition (Zhang et al. 2015, Meng et al. 2015, Li et al. 2015, Plouffe et al. 2016). We have now shown that STK25 is responsible for at least a portion of this remaining LATS activity,

and that the mechanism through which it promotes LATS activity is novel and independent from other upstream Hippo kinases. This may explain the robustness with which loss of this singular kinase is able to potently activate YAP. Further, this lack of mechanistic redundancy may also explain why STK25 appears to be frequently focally deleted in a spectrum of human cancers, which is not observed with members of the MST/MAP4K signaling cascade (Figure S6B).

Several questions remain regarding the regulation of Hippo signaling, especially with respect to how stimulatory inputs that induce loss of cytoskeletal tension ultimately activate kinases upstream of LATS (Zhou et al. 2009, Zheng et al. 2015, Meng et al. 2015). While the activation of MAP4K proteins is poorly understood, MST1/2 are activated by both the TAO family kinases and through auto-phosphorylation events (Praskova et al. 2004, Boggiano et al. 2011, Poon et al. 2011), suggesting STK25 may be subject to similar regulatory control. Alternatively, STK25 may be constitutively active and loss of cytoskeletal tension simply promotes LATS-STK25 interaction. Indeed, it was recently shown that TRIP6 negatively regulates LATS by competing for MOB1 binding, and that this inhibition of LATS is relieved upon loss of cytoskeletal tension, suggesting that loss of tension allows for recruitment of LATS to other binding partners that promote its activity (Dutta et al. 2018). Another possibility involves spatial regulation of STK25 in tandem with the status of the Golgi apparatus. STK25 is known to localize to and regulate the polarization of the Golgi ribbon (Preisinger et al. 2004, Matsuki et al. 2010). Recent studies have implicated the Golgi as serving a sensor role that integrates extracellular signals for signaling pathways regulating cellular proliferation (Thomas et al. 2014). It is possible that when the Golgi becomes disorganized under conditions of low cytoskeletal tension, such as when a cell becomes contact inhibited or actin becomes pharmacologically disrupted (Lazaro-Dieguez et al. 2006), that STK25

becomes released from the Golgi to associate with LATS kinases. Alternatively, loss of tension and consequent Golgi disruption may serve as a signal to recruit LATS kinases to sites of disturbed Golgi, where they can then associate with STK25 to promote LATS activity.

In conclusion, we define STK25 as a novel regulator of Hippo signaling, which activates LATS1/2 via a novel mechanism independent from the canonical MST/MAP4K signaling pathway. The novelty of this mechanism explains why loss of this single kinase is able to induce significant activation of YAP, which is unable to be compensated for by the presence of other upstream Hippo kinases. We posit that *STK25* is a putative tumor suppressor gene, with data from human cancers supporting our claim; *STK25* appears to undergo significant focal deletions in a large variety of human cancers, and loss of STK25 in our cellular models promotes increased proliferation and resistance to stimuli that would normally induce cell cycle arrest. Deletions or mutations of core Hippo pathway components are rare, and it remains to be discovered how cancer cells overcome this critical tumor suppressor pathway in the process of transformation. Our data demonstrate that loss of STK25 represents one potential route through which cancer cells might deregulate this critical tumor suppressor pathway to achieve pathologic capacity.

Materials and Methods

Cell culture

HEK293A cells were obtained from Invitrogen. 293FT, hTERT-RPE-1, and IMR90 fibroblasts were purchased from ATCC. HEK293A and IMR90 were cultured in high glucose DMEM (Gibco) supplemented with 10% Fetal Bovine Serum (ThermoFisher) with 100 IU/mL Penicillin and 100 µg/mL Streptomycin (ThermoFisher). For all experiments involving IMR90 fibroblasts, cells

between passages 11 and 17 were used. 293FT and hTERT-RPE-1 were cultured in DME/F12 supplemented with 10% FBS and 100 IU/mL Penicillin and 100 µg/mL Streptomycin. STK25 transgenic MEFs were provided by Dr. Brian Howell of SUNY Upstate, and were cultured in high glucose DMEM supplemented with 10% FBS, 100 IU/mL Penicillin, 100 µg/mL Streptomycin, 1X concentration of Non-Essential Amino Acids (Gibco), and 1 mM Sodium Pyruvate (Gibco). For all experiments involving MEFs, cells between passages 2 and 5 were used, and all samples were appropriately passage matched between different genotypes. Wild-type, MM8KO, and LATS dKO HEK293A were generous gifts from Kun-Liang Guan, and were cultured in high glucose DMEM (Gibco) supplemented with 10% Fetal Bovine Serum (ThermoFisher) with 100 IU/mL Penicillin and 100 µg/mL Streptomycin (ThermoFisher). All cells were maintained at 37ºC with a 5% CO_2 atmosphere.

Cell culture analysis

IMR90 fibroblasts were transfected with siRNA pools directed against individual kinase members of the Sterile20 superfamily of kinases. 48 hours post-transfection, these fibroblasts were treated with 10 µM Dihydrocytochalasin B (DCB) for 1 hour to acutely induce loss of actin cytoskeletal tension and thereby activate Hippo signaling. Protein lysates were then collected and levels of YAP phosphorylation were assessed via quantitative immunoblotting. A total of three independent replicates were performed to obtain a list of kinases which reduced YAP phosphorylation under DCB treatment in these cells. The top four hits were then knocked down via siRNA transfection again in hTERT-RPE-1 cells, and DCB treatment was performed again as before. Quantitative immunoblotting was performed on RPE-1 lysates to assess YAP phosphorylation; a total of four independent replicates were performed. To further assess the effects of STK25 loss in HEK293A

cells, Hippo signaling was activated by treatment with either 10 μM DCB or 1 μg/mL Latrunculin A for 1 hour to acutely disrupt the actin cytoskeleton, after which proteins were collected for downstream immunoblotting applications. To prevent other Hippo activating stimuli under conditions of pharmacologic actin disruption, cells were plated so that they would be sub-confluent at the time of DCB or Latrunculin A treatments. To activate Hippo signaling physiologically, cells were either grown to confluence, or were trypsinized and placed into cell culture media in a conical tube and incubated in suspension with end-over-end rocking to prevent adhesion. Protein samples were collected as before for immunoblotting applications. DCB was obtained from Sigma-Aldrich. Latrunculin A was obtained from Tocris Bioscience.

Generation of STK25 expression vectors, LentiCRISPR-STK25 vectors, and stable cell lines

Retroviral pWZL Blast Myc vector was a gift from William Hahn (Addgene, 10674) and bacterial expression vector pLDNT7 NFLAG-STK25 was obtained from DNASU (HsCD00298674). Both vectors were digested with BamHI and XhoI restriction enzymes (New England Biolabs) and fragments of interest were agarose gel purified. The NFLAG-STK25 insert was ligated into linearized pWZL Blast vector using T4 DNA ligase and transformed into DH5-Alpha chemically competent *E. coli*. Colonies were screened for inserts of correct size via restriction enzyme digest and the presence of gene of interest was verified by Sanger sequencing. To generate the kinase-dead STK25 expression vector, Lysine 49 of STK25 was mutated to an Arginine using cDNA sequence specific primers and Q5 Site-Directed Mutagenesis kit from New England Biolabs, and the presence of the correct mutation, as well as the absence of other mutations were confirmed via Sanger sequencing. For generation of STK25-targeting all-in-one CRISPR lentiviral vectors to concurrently express Cas9 and gRNA, two sgRNA targeting STK25 (sgRNA 1: 5'-

TGGATCATCATGGAGTACCTGGG-3'; sgRNA 2: 5'- TATGTCTCCTCCAGGGGACCTGG -3') were inserted into lentiCRISPR v2 (Addgene, 52961). A lentiCRISPR v2 vector with a non-targeting sgRNA sequence served as control. To generate viral particles, 293FT cells were transiently transfected with either retroviral or lentiviral vectors encoding genes of interest alongside appropriate packaging plasmids, after which cell culture supernatant was collected via centrifugation and sterile filtration. Viral infections were performed by incubating cells with viral supernatant alongside 10 µg/mL polybrene (Santa Cruz Biotechnology) for 16 hours, after which cells were allowed to recover for 24 hours prior to application of antibiotic selection with either 5 µg/mL of Blasticidin (Sigma-Aldrich) or 4 µg/mL of Puromycin (Santa Cruz Biotechnology), depending on the viral vector being used. For overexpression experiments, pools of stably infected cells were collected and used, while further single cell cloning with cloning cylinders (Fisher Scientific) were performed for experiments involving CRISPR-Cas9 knockout cell lines.

Plasmids and transfections

pWZL Blast GFP was from Robert Weinberg (Addgene, 12269). pWZL Blast Myc was from William Hahn (Addgene, 10674). pcDNA3.1 FLAG-MAP4K1 was a generous gift from Duojia Pan. pcDNA3.1 FLAG-HA was from Adam Antebi (Addgene 52535). LATS expression vectors were described previously (Ganem et al. 2014). Cells were plated at a density of 60-70% confluence prior to transfection and allowed to adhere overnight. For siRNA transfections, 50 nM of siRNA were transfected using Lipofectamine RNAiMAX (ThermoFisher Invitrogen) according to the manufacturer's instructions. For DNA transfections, plasmid DNA were transfected using Lipofectamine 3000 (ThermoFisher Invitrogen) according to the manufacturer's instructions. Cells were harvested for downstream applications 48-72 hours post-transfection. Please refer to

Supplemental Table 1 for a list of all siRNA oligonucleotide sequences used for this study.

Synthetic YAP/TAZ Luciferase Reporter Assay

HEK293A cells were plated in technical triplicates for each treatment group in a 96-well plate and transfected with siRNAs of interest as before. 24 hours post-siRNA transfection, cells were transfected with both the 8X GTIIC Luciferase reporter vector and the pRL-TK renilla luciferase vector using FuGENE HD transfection reagent (Promega) according to manufacturer's instructions. 8X GTIIC Luciferase was a generous gift from Bob Varelas. pRL-TK was obtained from Promega (E2241). 24 hours post-DNA transfection, cells were lysed in passive lysis buffer and luciferase activity levels were assessed using the Pierce Firefly Luciferase Glow and the Pierce Renilla Luciferase Glow kits according to manufacturer's instructions. Firefly luciferase activity levels were normalized to levels of Renilla luciferase activity in each well. A total of three independent experiments were performed and results are reported as mean ± SEM.

Protein extraction, immunoprecipitation, and quantitative immunoblotting

Cells were rinsed twice with ice-cold 1X PBS (Boston Bioproducts) and lysed immediately with 1X Cell Lysis Buffer (2% w/v SDS, 10% Glycerol, 60 mM Tris-HCl) supplemented with 1X HALT protease and phosphatase dual inhibitor cocktail (ThermoFisher). Cell lysates were then sonicated for 15 seconds at 20 kHz and Sample Buffer (Boston Bioproducts) was added to a final concentration of 1X, after which protein samples were incubated at 95ºC for 5 minutes. For immunoprecipitation experiments, cells were rinsed twice with ice-cold PBS as before and lysed with a standard IP Lysis Buffer (20 mM Tris-HCl, 150 mM NaCl, 1 mM EDTA, 1mM EGTA, 1% Triton X-100, 1 mM β-Glycerophosphate, 1 mM Sodium Orthovanadate) supplemented with a

protease inhibitor tablet (Sigma-Aldrich). Lysates were then transferred to microfuge tubes and centrifuged at 17,000 x G for 10 minutes to collect insoluble pellets. The supernatants containing soluble proteins were used for downstream applications. Cell lysates were resolved via SDS-PAGE and transferred to PVDF membranes (Bio-Rad) using a TransBlot Turbo semi-dry transfer system (Bio-Rad). Following transfer, membranes were blocked in TBS-0.5% Tween-20 (10 mM Tris-HCl, 150 mM NaCl, 0.5% Tween-20) containing 5% non-fat dried milk (NFDM) for 1 hour, and then incubated with primary antibodies diluted in 1% NFDM TBS-0.5% Tween-20 solution. The antibodies used for quantitative immunoblotting were the following: anti-LATS1 (1:1000, Cell Signaling Technology, 3477), anti-LATS2 (1:500, Cell Signaling Technology, 5888), anti-YAP (1:1000, Cell Signaling Technology, 14074), anti-P-YAP S127 (1:1000, Cell Signaling Technology, 13008), anti-P-YAP S397 (1:1000, Cell Signaling Technology, 13619), anti-STK25 (1:5000, Abcam, ab157188), anti-GAPDH (1:5000, Cell Signaling Technology, 2118), anti-P-LATS T1079 (1:500, Cell Signaling Technology 8654), anti-P-LATS S909 (1:500, Cell Signaling Technology, 9157), anti-FLAG (1:1000, Sigma, P2983), anti-MAP4K1 (1:5000, Abcam, ab33910), and anti-α-Tubulin (1:10000, Millipore, CP06-100UG). Primary antibodies were detected using horseradish peroxidase-conjugated species-specific secondary antibodies and ECL Prime (GE Amersham), Clarity ECL blotting substrate (Bio-Rad) or Clarity Max ECL blotting substrate (Bio-Rad). Imaging of blots were performed using the ChemiDoc XRS+ imaging system (Bio-Rad), and quantitative densitometry was performed using the Bio-Rad ImageLab software. For immunoprecipitations, proteins of interest were precipitated using Protein G magnetic beads (New England Biolabs) and either anti-FLAG (Sigma-Aldrich, P2983), anti-HA (Abcam, ab18181) or anti-Myc (ThermoFisher, MA1-33272) primary antibodies. Following pulldown of protein targets, magnetic beads were washed three times with ice-cold IP lysis buffer and then eluted using 2X

Sample Buffer by incubating at 95ºC for 5 minutes. Eluted proteins were then assessed via SDS-PAGE. Phos-tag electrophoresis was performed according to manufacturer's instructions, using the manganese reagent option (Wako Chemicals, AAL-107).

In Vitro Kinase Assay

Cells transfected with either FLAG-STK25, FLAG-MAP4K1, or HA-LATS2 were lysed in ice-cold modified cell lysis buffer, (25 mM Tris-HCl, 150 mM NaCl, 1 mM EDTA, 1 mM EGTA, 1% Triton X-100) supplemented with a protease inhibitor tablet, and incubated on ice for 30 minutes with occasional agitation. The supernatant containing soluble proteins was collected via centrifugation, and immunoprecipitation was performed as described above. Pellets containing immunoprecipitated proteins of interest were washed three times with ice-cold modified cell lysis buffer, and then three times with ice-cold *in vitro* kinase assay buffer (25 mM Tris-HCl, 1 mM β-Glycerophosphate, 1 mM Sodium Orthovanadate, 10 mM Magnesium Chloride, 10 mM DTT) supplemented with a protease inhibitor tablet. *In vitro* kinase assays were then performed by mixing the pellets containing immunoprecipitated FLAG-STK25 or FLAG-MAP4K1 together with pellets containing immunoprecipitated HA-LATS2 in a microfuge tube and incubating the mixture at 30ºC for 30 minutes in the presence of 500 µM ATP. Reactions were terminated by the addition of 2X Sample Buffer and incubating the mixture at 95ºC for 5 minutes, and samples were assessed via SDS-PAGE and immunoblotting for LATS phosphorylation.

Immunofluorescence Microscopy

Cells were washed once with PBS and fixed with 4% paraformaldehyde (Electron Microscopy Sciences) for 15 minutes. Cells were then extracted with TBS-0.5% Triton X-100 for 5 minutes,

blocked in TBS-BSA (10 mM Tris-HCl, 150 mM NaCl, 5% Bovine Serum Albumin, 0.2% Sodium Azide) for 30 minutes at room temperature, and incubated with primary antibodies diluted in TBS-BSA for 1 hour in a humidified chamber. The following antibodies and reagents were used: anti-YAP 63.7 (1:250, Santa Cruz Biotechnology, sc-6864), anti-YAP65 (1:200, Abcam, 2060-1), anti-α-Tubulin (1:1000, Millipore, CP06-100UG), and anti-FLAG (1:250, Sigma, P2983). Bound primary antibodies were visualized using species-specific fluorescent secondary antibodies (1:250, Molecular Probes, A11001, 11005, A11008), while DNA was visualized using 2.5 µg/mL Hoechst; F-actin was visualized using rhodamine conjugated phalloidin (1:500, Molecular Probes, R415). Immunofluorescence images were obtained using a Nikon TE2000-E2 inverted microscope. Images were analyzed using NIS-Elements software. For quantifications of YAP subcellular localization, two boxes of equal size were drawn in individual cells: one in the nucleus, and one in the cytoplasm. The mean fluorescence intensity of YAP was measured in these regions of interest and a nuclear:cytoplasmic ratio was determined. All quantifications of immunofluorescent images were performed in a blinded fashion. To assess rescue of tetraploidy-induced cell cycle arrest via an EdU incorporation assay, hTERT-RPE-1 cells were plated onto glass coverslips and transfected with siRNAs of interest. At 24 hours post-transfection, cells were treated with 4 µM DCB for 16 hours, and then washed four times with cell culture media and allowed to recover for a further 24 hours. Cells were then pulsed with 10 µM EdU (ThermoFisher) for 2 hours in fresh media and then immediately fixed in 4% paraformaldehyde. EdU incorporation was visualized using the Click-iT EdU Alexa Fluor 488 kit (ThermoFisher, C10337) as per manufacturer's instructions. DNA was stained using 2.5 µg/mL Hoechst as before. Coverslips were imaged and binucleated cells were scored as being positive if EdU signal was present in both nuclei.

RNA Extraction, Generation of cDNA, and qRT-PCR

Total RNA from cultured cells were extracted using the RNeasy kit (Qiagen), and cDNA was generated from RNA using the Superscript III kit and oligo(dT) primers (Invitrogen). Quantitative real-time PCR was performed using SYBR Green reagents in a StepOnePlus system (Applied Biosystems). Please refer to Supplemental Table 2 for a list of all primers for real-time PCR used in this study.

Microarray Analysis and Gene Set Enrichment Analysis

Total RNA was extracted from exponentially growing RPE-1 cells at 72-hours post-transfection with the RNeasy kit (Qiagen) and was hybridized onto Affymetrix HG-U133_Plus_2 arrays according to the manufacturer's instructions. For Gene Set Enrichment Analysis, a rank-ordered list of genes from the siSTK25 group relative to controls was used as input for preranked GSEA using the meandiv method for normalization and a weighted enrichment statistic. Microarray data have been deposited under the accession code GSEXXXXXXX.

Live Cell Imaging

To assess rescue of contact inhibition-mediated cell cycle arrest following siRNA transfection, hTERT-RPE-1-FUCCI cells were grown on glass-bottom 12-well tissue culture dishes (Mattek) and transfected with siRNAs of interest. At 24 hours post-transfection, imaging began on a Nikon TE2000-E2 inverted microscope equipped with the Nikon Perfect Focus system. The microscope was enclosed within a temperature and atmosphere-controlled environment at 37ºC and 5% humidified CO_2. Fluorescence and phase contrast images were captured every 15 minutes with a 10X 0.5 NA Plan Fluor objective at multiple points for 72 hours. All captured images were

quantified using NIS-Elements software in a blinded fashion.

Cell Proliferation Assay

Each clonal HEK293A cell line was seeded into 6-well plates at a density of 2.5×10^4 cells per well, and one well was trypsinized and counted every 48 hours, for a total of five total time points. A total of three independent experiments was performed, and data is presented as mean ± SEM for each clonal cell line.

Analysis of TCGA Datasets

Focal deletions of STK25 were analyzed using the Tumorscape online program through the Broad Institute (http://portals.broadinstitute.org/tcga/home) using Gene-Centric GISTIC analysis; the dataset used was the "2015-06-01 stddata_2015_04_02_regular peel-off." To assess levels of focal deletion of other identified upstream Hippo kinases, the same dataset was probed for other MSTs as well as members of the MAP4K family. To assess clinical outcomes in sarcoma patients with deletions in STK25, the TCGA dataset for Sarcomas was assessed and analyzed using the UCSC Xena Functional Genomics Browser (https://xenabrowser.net/). Patients were scored as having deletions of STK25 based on GISTIC-thresholded reads of STK25 gene copy number; if such copy numbers were either -1 or -2, then the patients were scored as having deletions of STK25. Patients with normal copy numbers of STK25 (0) or amplifications (1 or 2) were concatenated into one group for the purposes of survival analysis.

Quantification and Statistical Analysis

All quantitative data have been presented as mean ± SEM, unless otherwise indicated. The number

of samples (n) represent the number of biologic replicates, except in the case of immunofluorescent image quantifications, in which they represent the number of cells quantified per group of interest over three or more biologic replicates. Prism 7 was used for all statistical analyses. Data were subjected to the D'Agostino-Pearson normality test to determine whether standard parametric tests should be applied to test for significant differences between groups. Data passing the normality test, or data with insufficient data points to conclusively assess normality were assessed via parametric tests of significance. Data failing the normality test were assessed using non-parametric tests of significance. Experiments in which more than two independent groups were assessed simultaneously, ANOVA with the appropriate post-hoc tests of significant differences were applied. Linear associations, where appropriate, were assessed using Pearson's correlation coefficient. For assessment of statistical differences between cellular proliferation curves, a two-way ANOVA with Tukey's post-hoc analysis was performed. Kaplan-Meier survival analysis of sarcoma patients with *STK25* deletions were performed using the log-rank test. Statistical tests with p-values of <0.05 were considered significant.

Acknowledgments

We would like to thank Kun-Liang Guan and members of his lab for technical advice and cell lines, Duojia Pan for reagents, and Bob Varelas and Anurag Singh for critical discussions about the work. We would also like to thank members of the Ganem lab for detailed comments on the manuscript. S.L is supported by a Medical Student Research Grant from the Melanoma Research Foundation and a Medical Student Young Investigator Award from the American Skin Association. M.V. is supported by a training grant from the NIH/NIGMS (5T32GM008541-20) and an F30 Award from the NCI (1F30CA228388-01). R.Q. is supported by a Canadian Institutes of Health Research

Doctoral Foreign Study Award. B.H. is supported by NIH grant NS073662. N.G is a member of the Shamim and Ashraf Dahod Breast Cancer Research Laboratories and is supported by NIH grants CA154531 and GM117150, the Karin Grunebaum Foundation, the Smith Family Awards Program, the Melanoma Research Alliance, and the Searle Scholars Program.

Author Contributions

S.L., H.C., and N.J.G. conceptualized and designed the study. S.L. performed experiments with R.J.Q. for bioinformatic analysis of datasets and with T.M., H.M.M., M.A.V., and I.P.M.M. for all other experiments. S.L. and N.J.G. analyzed the results. B.W.H. provided critical reagents. S.L. and N.J.G. wrote the manuscript. All authors commented on the manuscript.

References

1. Adler JJ, Johnson DE, Heller BL, Bringman LR, Ranahan WP, Conwell MD, Sun Y, Hundmon A, Wells CD. 2013. Serum deprivation inhibits the transcriptional co-activator YAP and cell growth via phosphorylation of the 130-kDa isoform of Angiomotin by the LATS1/2 protein kinases. *Proc Natl Acad Sci* **110**:17368-73.
2. Boggiano JC, Vanderzalm PJ, Fehon RG. 2011. Tao-1 phosphorylates Hippo/MST kinases to regulate the Hippo-Salvador-Warts tumor suppressor pathway. *Dev Cell* **21**: 888-895.
3. Dupont S, Morsut L, Aragona M, Eno E, Giulitti S, Cordenonsi M, Zanconato F, Le Digabel J, Forcato M, Bicciato S, Elvassore N, Piccolo S. 2011. Role of YAP/TAZ in mechanotransduction. *Nature* **474**:179-183.
4. Dutta S, Mana-Capelli S, Paramasivam M, Dasgupta I, Cirka H, Billiar K, McCollum D. 2018. TRIP6 inhibits Hippo signaling in response to tension at adherens junctions. *EMBO Rep.* **19**: 337-350.
5. Enzo E, Santinon G, Pocaterra A, Aragona M, Bresolin S, Forcato M, Grifoni D, Pession A, Zanconato F, Guzzo G, Bicciato S, Dupont S. 2015. Aerobic glycolysis tunes YAP/TAZ transcriptional activity. *EMBO J*. **34**: 1349-1370.
6. Fernandez-L A, Northcott PA, Dalton J, Fraga C, Ellison D, Angers S, Taylor MD, Kenney AM. 2009. YAP1 is amplified and up-regulated in hedgehog-assisted medulloblastomas and mediates Sonic hedgehog-driven neural precursor proliferation. *Genes Dev.* **23**: 2729-2741.
7. Ganem NJ, Cornils H, Chiu SY, O'Rourke KP, Arnaud J, Yimlamai D, Théry M, Camargo FD, Pellman D. 2014. Cytokinesis failure triggers hippo tumor suppressor pathway activation. *Cell*. **158**:833-848.
8. Hoa L, Kulaberoglu Y, Gundogdu R, Cook D, Mavis M, Gomez M, Gomez V, Hergovich A.

2016. The characterisation of LATS2 kinase regulation in Hippo-YAP signalling. *Cell Signal.* **28**: 488-497.

9. Hong JH, Hwang ES, McManus MT, Amsterdam A, Tian Y, Kalmukova R, Mueller E, Benjamin T, Spiegelman BM, Sharp PA, Hopkins N, Yaffe MB. 2004. TAZ, a transcriptional modulator of mesenchymal stem cell differentiation. *Science*. **309**:1074-1078.
10. Kelliher FC, O'Sullivan H. 2013. Oxford and the Savannah: Can the Hippo Provide and Explanation for Peto's Paradox? *Clin Cancer Res*. **20**:1-8.
11. Kim MH, Kim J, Hong H, Lee JK, Jung E, Kim J. 2016. Actin remodeling confers BRAF inhibitor resistance to melanoma cells through YAP/TAZ activation. *EMBO J*. **35**:462-78.
12. Lazaro-Dieguez F, Jimenez N, Barth H, Koster AJ, Renau-Piqueras J, Llopis JL, Burger KN, Egea G. 2006. Actin filaments are involved in the maintenance of Golgi cisternae morphology and intra-Golgi pH. *Cell Motil Cytoskeleton* **63**: 778-791.
13. Li Q, Li S, Mana-Capelli S, Roth Flach RJ, Danai LV, Amcheslavsky A, Nie Y, Kaneko S, Yao X, Chen X, Cotton JL, Mao J, McCollum D, Jiang J, Czech MP, Xu L, Ip YT. 2014. The conserved misshapen-warts-Yorkie pathway acts in enteroblasts to regulate intestinal stem cells in Drosophila. *Dev. Cell* **31**: 291-304.
14. Li S, Cho YS, Yue T, Ip YT, Jiang J. 2015. Overlapping functions of the MAP4K family kinases Hppy and Msn in Hippo signaling. *Cell Discov.* **1**: 15038.
15. Li W, Cooper J, Zhou L, Yang C, Erdjument-Bromage H, Zagzag D, Snuderl M, Ladanyi M, Hanemann CO, Zhou P, Karajannis MA, Giancotti FG. 2014. Merlin/*NF2* Loss-Driven Tumorigenesis Linked to $CRL4^{DCAF1}$-Mediated Inhibition of the Hippo Pathway Kinases Lats1 and 2 in the Nucleus. *Cancer Cell* **14**: 48-60.
16. MacLean-Fletcher S, Pollard TD. 1980. Mechanism of action of cytochalasin B on actin. *Cell*

20:329-341.

17. Matsuki T, Matthews RT, Cooper JA, van der Brug MP, Cookson MR, Hardy JA, Olson EC, Howell BW. 2010. Reelin and stk25 have opposing roles in neuronal polarization and dendritic Golgi deployment. *Cell* **143**:826-836.
18. Meng Z, Moroishi T, Guan KL. 2016. Mechanisms of Hippo pathway regulation. *Genes Dev* **30**:1-17.
19. Meng Z, Moroishi T, Mottier-Pavie V, Plouffe SW, Hansen CG, Hong AW, Park HW, Mo JS, Lu W, Lu S, Flores F, Yu FX, Halder G, Guan KL. 2015. MAP4K family kinases act in parallel to MST1/2 to activate LATS1/2 in the Hippo pathway. *Nat Commun.* **6**:8357.
20. Mo JS, Meng Z, Kim YC, Park HW, Hansen CG, Kim S, Lim DS, Guan KL. 2015. Cellular energy stress induces AMPK-mediated regulation of YAP and the Hippo pathway. *Nat Cell Biol*. **17**:500-510.
21. Mohseni M, Sun J, Lau A, Curtis S, Goldsmith J, Fox VL, Wei C, Frazier M, Samson O, OWng KK, Kim C, Camargo FD. 2014. A genetic screen identifies an LKB1-MARK signaling axis controlling the Hippo-YAP pathway. *Nat Cell Biol* **16**: 108-117.
22. Mori M, Triboulet R, Mohseni M, Schlegelmilch K, Shrestha K, Camargo FD, Gregory RI. 2014. Hippo signaling regulates microprocessor and links cell-density dependent miRNA biogenesis to cancer. *Cell* **156**: 893-906.
23. Morton WM, Ayscough KR, McLaughlin PJ. 2000. Latrunculin alters the actin-monomer subunit interface to prevent polymerization. *Nat Cell Biol* **2**: 376-378.
24. Ni L, Zheng Y, Hara M, Pan D, Luo X. 2015. Structural basis for Mob1-dependent activation of the core Mst-Lats kinase cascade in Hippo signaling. *Genes Dev* **29**: 1416-1431.
25. Nishio M, Sugimachi K, Goto H, Wan J, Morikawa T, Miyachi Y, Yakano Y, Hikasa H, Itoh T,

Suzuki SO, Kurihara H, Aishima S, Leask A, Sasaki T, Nakano T, Nishina H, Nishikawa Y, Sekido Y, Nakao K, Shin-Ya K, Mimori K, Suzuki A. 2016. Dysregulated YAP1/TAZ and TGF-β signaling mediate hepatocarcinogenesis in *Mob1a/1b*-deficient mice. *Proc Natl Acad Sci* **113**:E71-E80.

26. Overholtzer M, Zhang J, Smolen GA, Muir B, Li W, Sgroi DC, Deng CX, Brugge JS, Haber DA. 2006. Transforming properties of YAP, a candidate oncogene on the chromosome 11q22 amplicon. *Proc Natl Acad Sci* **103**:12405-12410.
27. Pan D. 2010. The hippo signaling pathway in development and cancer. *Dev Cell* **19**: 491-505.
28. Park YY, Sohn BH, Johnson RL, Kang MH, Shin JJ, Mangala LS, Kim JH, Yoo JE, Rodriguez-Aguayo C, Pradeep S, Hwang JE, Jang HJ, Lee HS, Rupaimoole R, Lopez-Berestein G, Jeong W, Park IS, Park YN, Sood AK, Mills GB, Lee JS. 2016. YAP1 and TAZ Activates mTORC1 Pathway by Regulating Amino Acid Transporters in hepatocellular carcinoma. *Hepatology* **63**: 159-172.
29. Plouffe SW, Meng Z, Lin KC, Lin B, Hong AW, Chun JV, Guan KL. 2016. Characterization of Hippo Pathway Components by Gene Inactivation. *Mol Cell* **64**:993-1008.
30. Poon CL, Lin JI, Zhang X, Harvey KF. 2011. The sterile 20-like kinase Tao-1 controls tissue growth by regulating the Salvador-Warts-Hippo pathway. *Dev Cell* **21**: 896-906.
31. Praskova M, Khoklatchev A, Ortiz-Vega S, Avruch J. 2004. Regulation of the MST1 kinase by autophosphorylation, by the growth inhibitory proteins, RASSF1 and NORE1, and by Ras. *Biochem J* **381**: 453-462.
32. Preisinger C, Short B, De Corte V, Bruyneel E, Haas A, Kopajtich R, Gettemans J, Barr FA. 2004. YSK1 is activated by the Golgi matrix protein GM130 and plays a role in cell migration through its substrate 14-3-3zeta. *J Cell Biol* **164**:1009-1020.

33. Stegert MR, Tamaskovic R, Bichsel SJ, Hergovich A, Hemmings BA. 2004. Regulation of NDR2 Protein Kinase by Multi-site Phosphorylation and the S100B Calcium-binding Protein. *J Biol Chem* **279**: 23806-23812.

34. Tamaskovic R, Bichsel SJ, Rogniaux J, Stegert MR, Hemmings BA. 2003. Mechanism of Ca^{2+}-mediated Regulation of NDR Protein Kinase through Autophosphorylation and Phosphorylation by an Upstream kinase. *J Biol Chem* **278**: 6710-6718.

35. Thomas JD, Zhang YJ, Wei YH, Cho JH, Morris LE, Wang HY, Zheng XF. 2014. Rab1A is an mTORC1 Activator and Colorectal Oncogene. *Cancer Cell* **26**: 754-769.

36. Thompson BJ, Sahai E. 2015. MST kinases in development and disease. *J Cell Biol* **210**:871-82.

37. Wang W, Xiao ZD, Li X, Aziz KE, Gan B, Johnson RL, Chen J. 2015. AMPK modulates Hippo pathway activity to regulate energy homeostasis. *Nat Cell Biol* **17**:490-499.

38. Wu S, Liu Y, Zheng Y, Dong J, Pan D. 2008. The TEAD/TEF family protein Scalloped mediates transcriptional output of the Hippo growth-regulatory pathway. *Dev Cell* **14**:388-98.

39. Yin F, Yu J, Zheng Y, Chen Q, Zhang N, Pan D. 2013. Spatial Organization of Hippo signaling at the plasma membrane mediated by the tumor suppressor Merlin/NF2. *Cell* **154**:1342-1355.

40. Yu FX, Zhao B, Panupinthu N, Jewell JL, Lian I, Wang LH, Zhao J, Yuan H, Tumaneng K, Li H, Fu XD, Mills GB, Guan KL. 2012. Regulation of the Hippo-YAP pathway by G-protein-coupled receptor signaling. *Cell* **150**:780-791.

41. Zanconato F, Cordenonsi M, Piccolo S. 2016. YAP/TAZ at the Roots of Cancer. *Cancer Cell* **29**:783-803.

42. Zanconato F, Forcato M, Battilana G, Azzolin L, Quaranta E, Bodega B, Rosato A, Bicciato S, Cordenonsi M, Piccolo S. 2015. Genome-wide association between YAP/TAZ/TEAD and AP-

1 at enhancers drives oncogenic growth. *Nat Cell Biol* **17**:1218-1227.

43. Zhang H, Liu CY, Zha ZY, Zhao B, Yao J, Zhao S, Xiong Y, Lei QY, Guan KL. 2009. TEAD transcription factors mediate the function of TAZ in cell growth and epithelial-mesenchymal transition. *J Biol Chem* **284**:13355-13362.
44. Zhang L, Ren F, Zhang Q, Chen Y, Wang B, Jiang J. 2008. The TEAD/TEF family of transcription factor Scalloped mediates Hippo signaling in organ size control. *Dev Cell* **14**:377-87.
45. Zhao B, Li L, Tumaneng K, Wang CY, Guan KL. 2010. A coordinated phosphorylation by Lats and CK1 regulates YAP stability through SCF(beta-TRCP). *Genes Dev* **24**:72-85.
46. Zhao B, Li L, Wang L, Wang CY, Yu J, Guan KL. 2012. Cell detachment activates the Hippo pathway via cytoskeleton reorganization to induce anoikis. *Genes Dev* **26**:54-68.
47. Zhao B, Wei X, Li W, Udan RS, Yang Q, Kim J, Xie J, Ikenoue T, Yu J, Li L, Zheng P, Ye K, Chinaiyan A, Halder G, Lai ZC, Guan KL. 2007. Inactivation of YAP oncoprotein by the Hippo pathway is involved in cell contact inhibition and tissue growth control. *Genes Dev* **21**:2747-2761.
48. Zheng Y, Wang W, Liu B, Deng H, Uster E, Pan D. 2015. Identification of Happyhour/MAP4K as Alternative Hpo/Mst-like Kinases in the Hippo Kinase Cascade. *Dev Cell* **34**:642-55.
49. Zhou D, Conrad C, Xia F, Park JS, Payer B, Yin Y, Lauwers GY, Thasler W, Lee JT, Avruch J, Bardeesy N. 2009. Mst1 and Mst2 maintain hepatocyte quiescence and suppress hepatocellular carcinoma development through inactivation of the Yap1 oncogene. *Cancer Cell* **19**: 425-438.

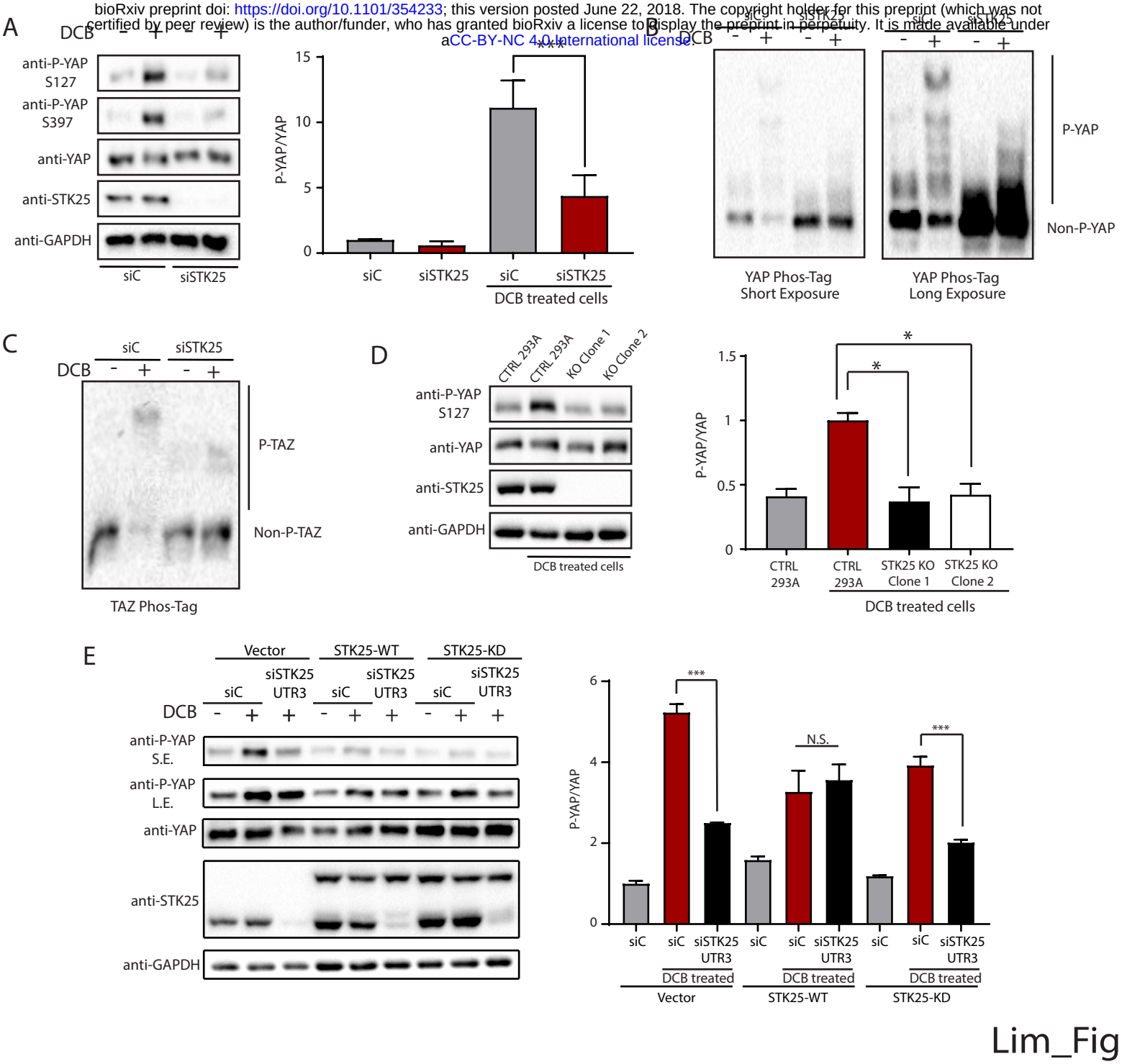

Lim_Fig1

Figure 1. STK25 regulates Hippo activation in response to loss of cytoskeletal tension.

(A) Immunoblot and quantitation of phosphorylated YAP levels following treatment with 10 μM DCB in HEK293A cells transfected with the indicated siRNA. (n=6; ***p<0.001, unpaired t-test). **(B)** Global phosphorylation status of YAP was assessed using Phos-tag gel electrophoresis following treatment with 10 μM DCB in HEK293A cells transfected with either control siRNA or STK25 siRNA. Shifted bands indicate degrees of YAP phosphorylation. **(C)** TAZ phosphorylation status was assessed using Phos-tag gel electrophoresis following treatment with 10 μM DCB in HEK293A cells transfected with either control siRNA or STK25 siRNA. **(D)** Immunoblot and quantitation of phosphorylated YAP levels following treatment with 10 μM DCB in either control HEK293A stably expressing Cas9 and a non-targeting sgRNA or STK25 KO 293A stably expressing Cas9 together with either sgRNA 1 (Clone 1) or sgRNA 2 (Clone 2) targeting STK25. (n=4; *p<0.05, One-way ANOVA with Dunnett's post-hoc analysis). **(E)** Immunoblot and quantitation of phosphorylated YAP levels following treatment with 10 μM DCB in HEK293A cells stably expressing wild-type STK25 (STK25-WT), kinase-dead STK25 (STK25-KD), or vector control (Vector) transfected with the indicated siRNAs. (n=3; ***p<0.001, N.S.: not significant; One-way ANOVA with Tukey's post-hoc analysis). S.E. stands for Short Exposure; L.E. stands for Long Exposure.

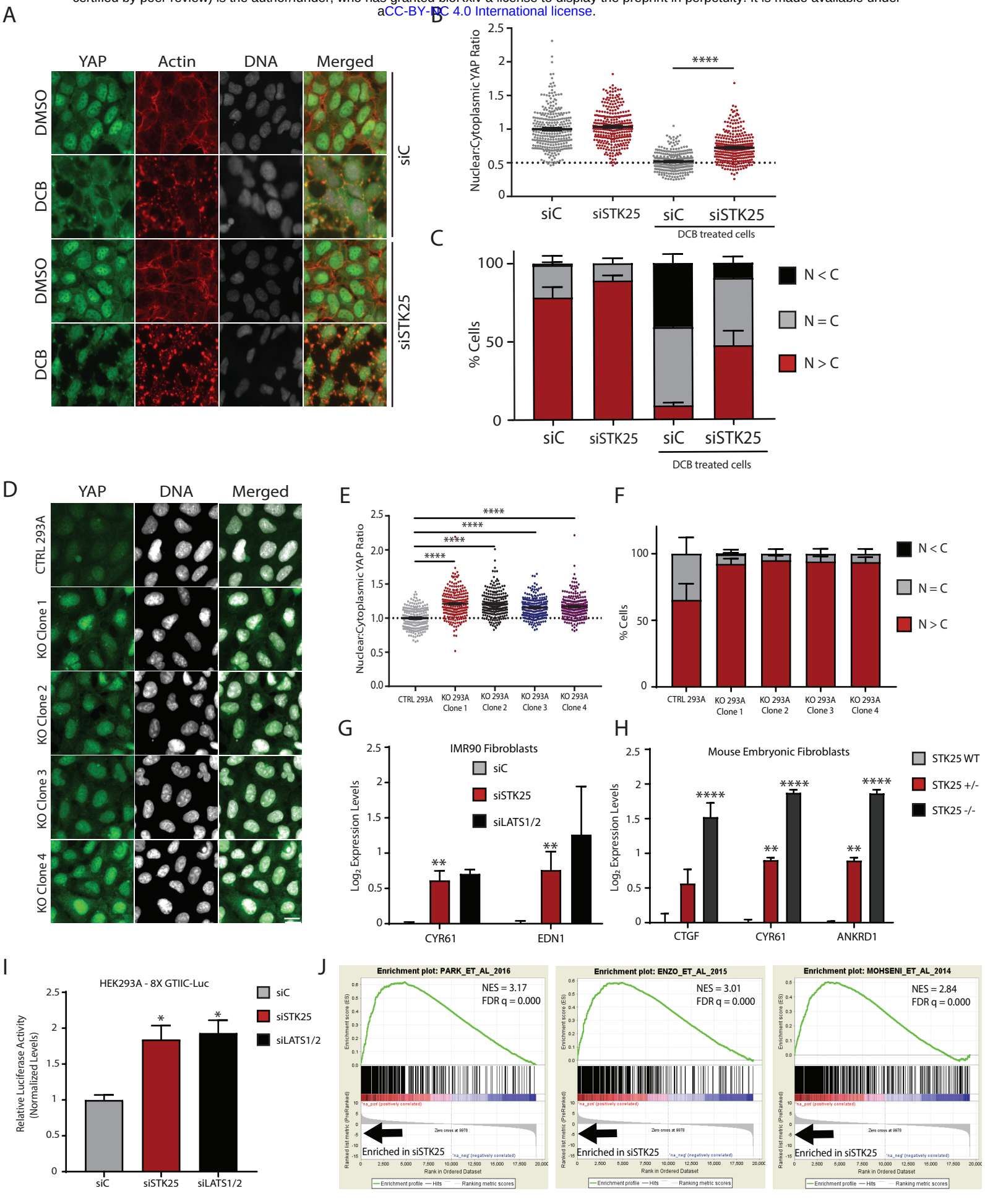

Lim_Fig2

Figure 2. Loss of STK25 promotes activation of YAP.

(A) HEK293A cells transfected with either control siRNA or STK25 siRNA stained for YAP (Green), Actin (Red), and DNA (White) following treatment with 5 μM DCB. Scale bar, 20 μm. **(B)** YAP intensity was quantified and nuclear:cytoplasmic ratios were calculated (n=225 per group over 3 biological replicates; ****p<0.0001, Mann-Whitney test). **(C)** YAP localization was quantified (n=3; N>C, YAP is enriched in the nucleus; N=C, YAP is evenly distributed between the nucleus and the cytoplasm; N<C, YAP is enriched in the cytoplasm). **(D)** Control and STK25 KO HEK293A were stained for YAP (Green) and DNA (White). Scale bar, 20 μm. **(E)** Nuclear:cytoplasmic YAP ratios of control and STK25 KO HEK293A were quantified (n=225 per group over 3 biological replicates; ****p<0.0001, Kruskal-Wallis test). **(F)** YAP localization in control and STK25 KO HEK293A was quantified as before (n=3 biological replicates). **(G)** qPCR analysis of YAP-target gene expression in IMR90 fibroblasts transfected with the indicated siRNA (n=4; **p<0.01, unpaired t-test). **(H)** qPCR analysis of YAP-target gene expression in wild-type, $STK25^{+/-}$, and $STK25^{-/-}$ mouse embryonic fibroblasts (n=3; **p<0.01, ****p<0.0001, One-way ANOVA with Dunnett's post-hoc analysis). **(I)** Expression of the TEAD luciferase reporter in HEK293A cells transfected with the indicated siRNA. Cells were transfected with siRNA, followed by transfection with 8X GTIIC TEAD luciferase reporter and pRL-TK renilla luciferase. Reporter luciferase activity was normalized to Renilla luciferase (n=3; *p<0.05, One-way ANOVA with Dunnett's post-hoc analysis). **(J)** An expression signature of genes most upregulated upon loss of STK25 was constructed and GSEA was performed against a curated list of publicly available active YAP/TAZ gene sets. The top three most enriched gene sets are shown here.

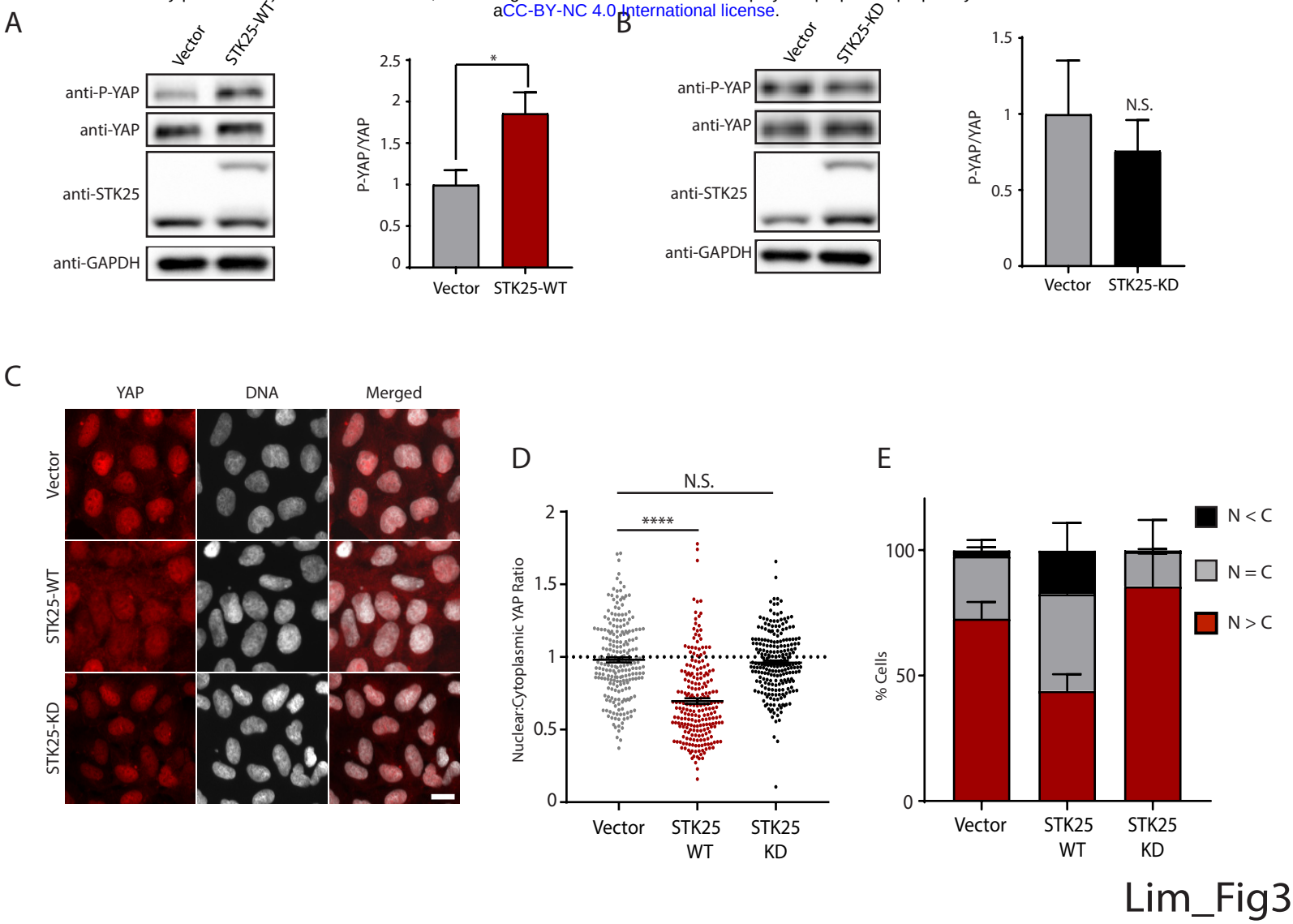

Lim_Fig3

Figure 3. Overexpression of STK25 promotes YAP phosphorylation.

(A) Immunoblot and quantitation of phosphorylated YAP levels in HEK293A cells stably expressing wild-type STK25 (STK25-WT) or vector control (Vector) (n=3; *p<0.05, paired t-test). **(B)** Immunoblot and quantitation of phosphorylation YAP levels in HEK293A cells stably expressing kinase-dead STK25 (STK25-KD) or vector control (Vector) (n=3; N.S. stands for not significant.) **(C)** HEK293A cells stably expressing STK25-WT, STK25-KD, or Vector were stained for YAP (Red) and DNA (White). Scale bar, 20 μm. **(D)** YAP intensities in Vector, STK25-WT, and STK25-KD HEK293A were quantified and nuclear:cytoplasmic ratios were calculated (n=225 per group over 3 biological replicates; ****p<0.0001, Mann-Whitney test). **(E)** YAP localization in Vector, STK25-WT, and STK25-KD HEK293A cells was quantified (n=3 biological replicates; N>C, YAP is enriched in the nucleus; N=C, YAP is evenly distributed between the nucleus and the cytoplasm; N<C, YAP is enriched in the cytoplasm).

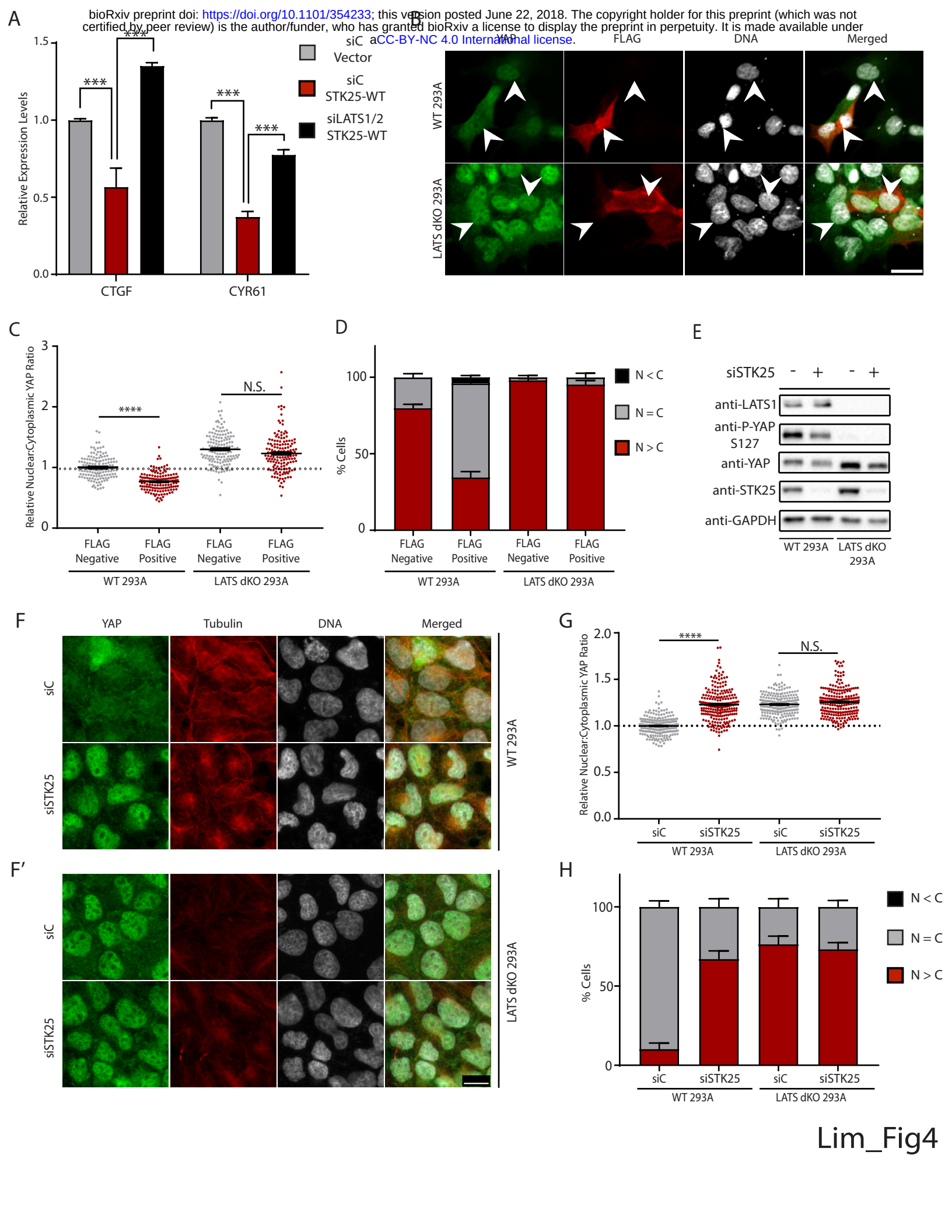

Lim_Fig4

Figure 4. STK25 acts through LATS1/2 to inhibit YAP.

(A) qPCR analysis of YAP-target gene expression in HEK293A cells stably overexpressing either wild-type STK25 (STK25-WT) or vector control (Vector) after transfection with control siRNA or siRNAs targeting LATS1 and LATS2 (n=3; ***p<0.001, One-way ANOVA with Tukey's post-hoc analysis). **(B)** Wild-type and LATS dKO HEK293A were transfected with a vector encoding FLAG-tagged wild-type STK25 and were stained for YAP (Green), FLAG (Red), and DNA (White). Arrows indicate representative cells selected for quantification that were positive for FLAG signal (indicating expression of transfected wild-type STK25) as well as an immediately adjacent cell negative of FLAG signal also selected for quantification to serve as controls. Scale bar, 20 μm. **(C)** YAP intensities were quantified in a FLAG-signal positive cell as well as a FLAG-signal negative cell immediately adjacent to it, and nuclear:cytoplasmic ratios were calculated (n=200 per group over 4 biological replicates; ****p<0.0001, Kruskal-Wallis test with Dunn's post-test; N.S. indicates "not significant.") **(D)** YAP localization in the FLAG-STK25-WT transfected wild-type and LATS dKO HEK293A were quantified (n=4 biological replicates; N>C, YAP is enriched in the nucleus; N=C, YAP is evenly distributed between the nucleus and the cytoplasm; N<C, YAP is enriched in the cytoplasm). **(E)** Representative immunoblot of phosphorylated YAP following STK25 knockdown in wild-type and LATS dKO HEK293A. Cells were grown to confluence in order to activate Hippo signaling to induce YAP phosphorylation. **(F)** Wild-type and LATS dKO HEK293A were transfected with either Control siRNA or STK25 siRNA and were allowed to grow to confluence. These cells were stained for YAP (Green), Tubulin (Red), and DNA (White). **(G)** YAP intensities were quantified and nuclear:cytoplasmic ratios were calculated (n=225 over 3 biological replicates; ****p<0.0001, Kruskal-Wallis test with Dunn's post-test; N.S. indicates "not significant.") **(H)** YAP localization in wild-type and LATS dKO

HEK293A transfected with Control siRNA or STK25 siRNA were quantified (n=3 biological replicates; N>C, YAP is enriched in the nucleus; N=C, YAP is evenly distributed between the nucleus and the cytoplasm; N<C, YAP is enriched in the cytoplasm).

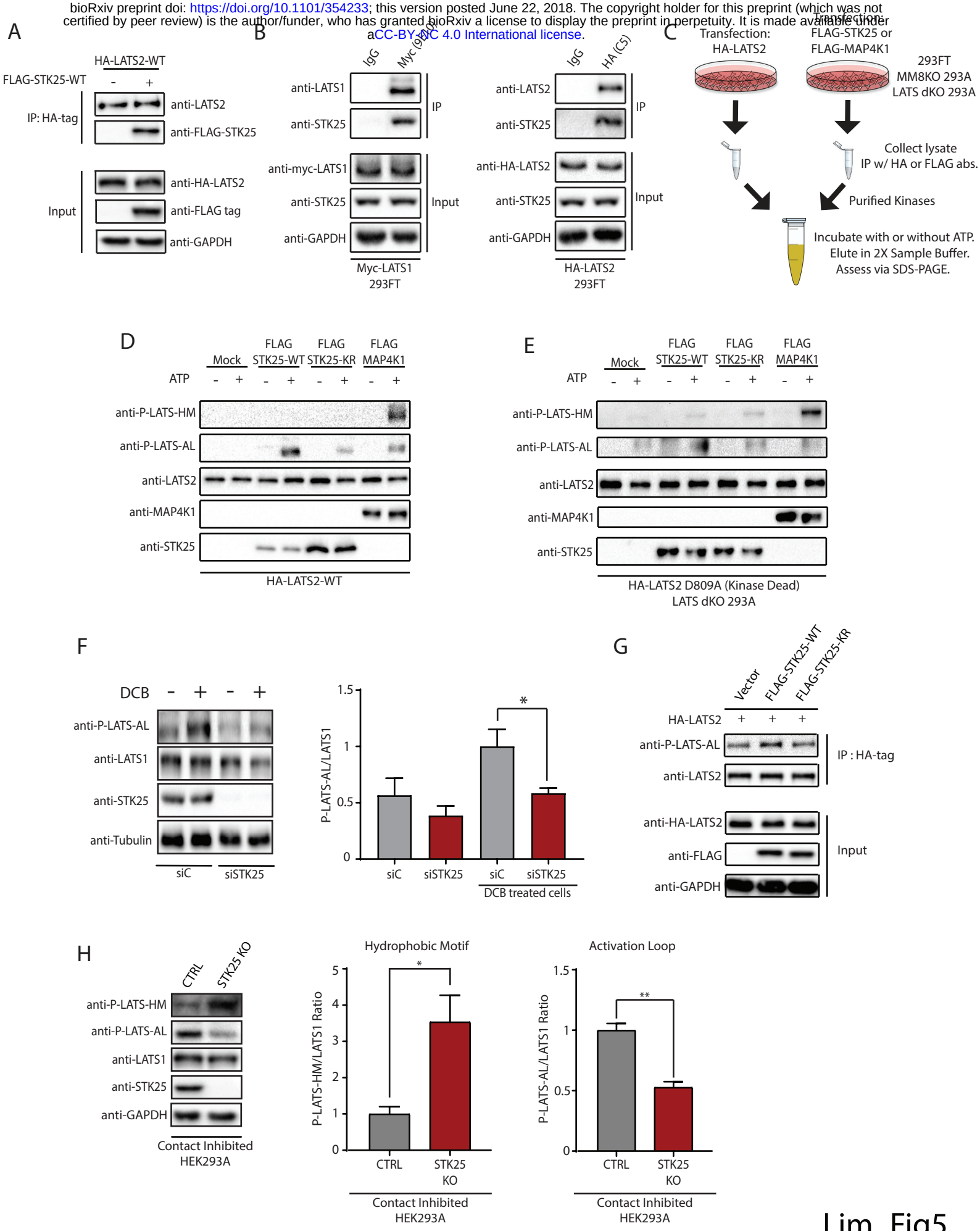

Lim_Fig5

Figure 5. STK25 directly phosphorylates the activation loop of LATS.

(A) HEK293A cells were transfected with HA-LATS2 and either vector control or FLAG-STK25. LATS2 was then immunoprecipitated with an antibody against HA. Co-precipitation of FLAG-STK25 with HA-LATS2 was assessed by immunoblotting. **(B)** Lysates were collected from HEK293A cells transfected with Myc-LATS1 or HA-LATS2. LATS1 and LATS2 were immunoprecipitated using antibodies directed against their tags (Myc or HA) and co-precipitation of endogenous STK25 was assessed by immunoblotting. IgG served as control for the IP reactions. **(C)** Schema of the *in vitro* kinase assay set-up. The indicated cell lines were transfected with HA-LATS2, FLAG-STK25, or FLAG-MAP4K1. Protein lysates were then collected from these cells and used to individually immunoprecipitate the kinases of interest. The purified kinases were then mixed together in kinase assay buffer and incubated for 30 minutes at 30°C with or without 500 μM ATP. Reactions were then terminated by the addition of sample buffer, and levels of LATS phosphorylation were assessed via immunoblotting. **(D)** Immunoprecipitation (IP) purified wild-type LATS2 (HA-LATS2-WT) was co-incubated with IP purified wild-type STK25 (FLAG-STK25-WT), kinase-dead STK25 (FLAG-STK25-KD), or wild-type MAP4K1 (FLAG-MAP4K1) either with or without 500 μM ATP and assessed for phosphorylation on its hydrophobic motif (P-LATS-HM) or activation loop motif (P-LATS-AL). A mock IP product from untransfected 293FT lysates using FLAG antibody and protein G magnetic beads served as control. **(E)** IP purified kinase-dead LATS2 (HA-LATS2-KD) from transfected LATS dKO 293A cells was co-incubated with IP purified FLAG-STK25-WT, FLAG-STK25-KD, or FLAG-MAP4K1, all from transfected LATS dKO 293A. Kinase reactions were allowed to occur either with or without 500 μM ATP, and levels of phosphorylated LATS at the hydrophobic motif (P-LATS-HM) and activation loop motif (P-LATS-AL) were assessed via immunoblotting. A mock IP product from untransfected LATS

dKO 293A lysates using FLAG antibody and protein G magnetic beads served as control. **(F)** Immunoblot and quantification of LATS activation loop phosphorylation (P-LATS-AL) following treatment with 10 μM DCB in HEK293A cells transfected with the indicated siRNA. (n=4; *p<0.05, paired t-test). **(G)** Lysates from HEK293A cells co-transfected with HA-tagged wild-type LATS2 (HA-LATS2-WT) and either vector control (Vector), wild-type STK25 (FLAG-STK25-WT), or kinase-dead STK25 (FLAG-STK25-KD) were used to immunoprecipitate HA-LATS2. Immunoprecipitated LATS2 was then used to assess levels of activation loop phosphorylation by immunoblotting. Input lysates were also assessed by immunoblotting for assessing protein loading and verification of transfected protein expression. **(H)** Immunoblot and quantification of LATS1 hydrophobic motif (P-LATS-HM) and activation loop (P-LATS-AL) phosphorylation in either control HEK293A stably expressing Cas9 and a non-targeting sgRNA or STK25 KO 293A stably expressing Cas9 together with sgRNA 1 grown to confluence (n=3; *p<0.05, **p<0.01, paired t-test).

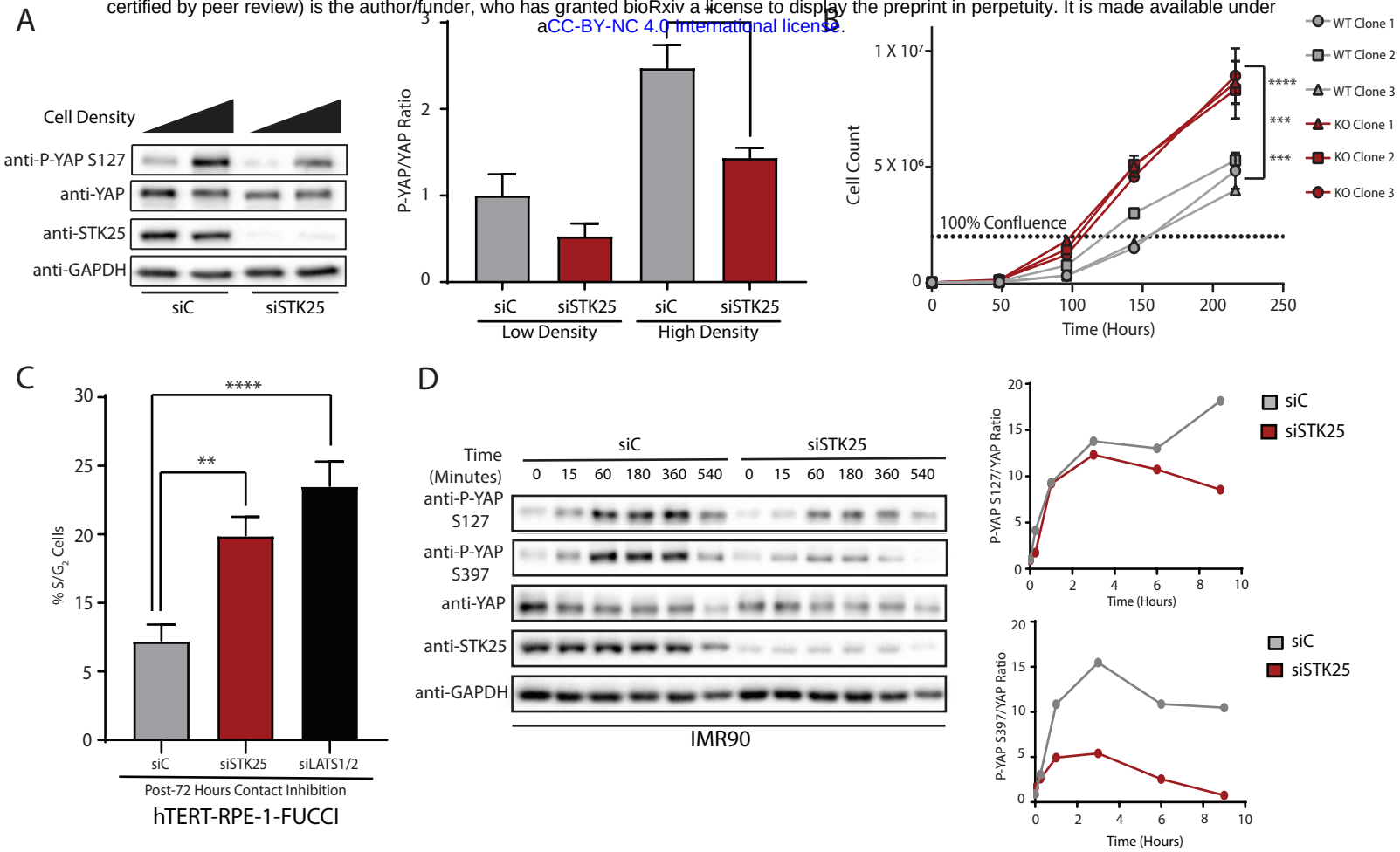

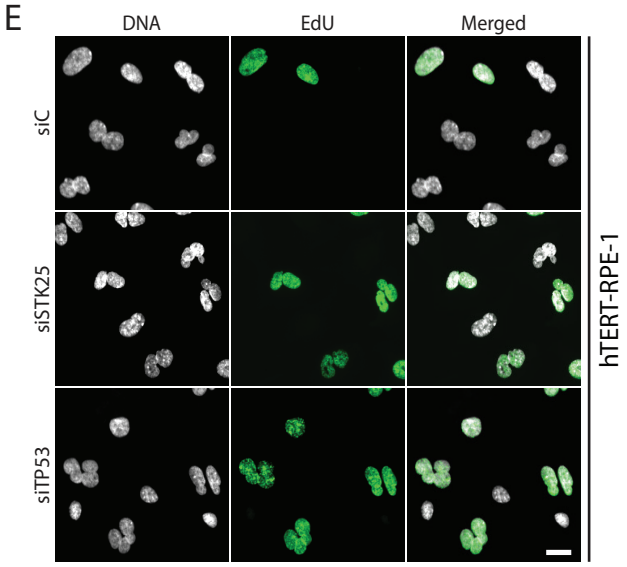

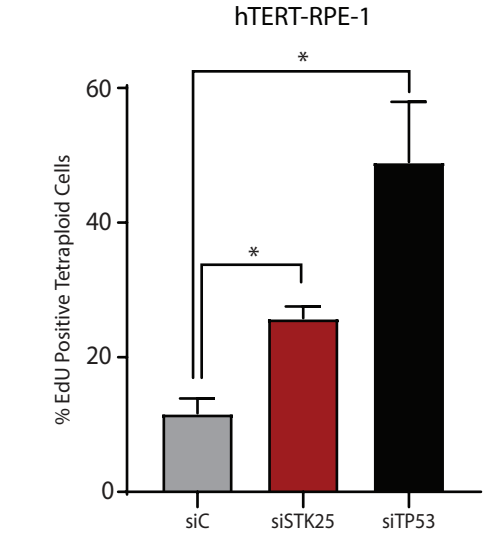

Lim_Fig6

Figure 6. STK25 regulates YAP phosphorylation in response to physiologic stimuli.

(A) Immunoblot and quantification of YAP phosphorylation in HEK293A cells grown to low confluence or high confluence after transfection with the indicated siRNA. (n=3; *p<0.05, unpaired t-test). **(B)** Cellular proliferation curves of control HEK293A clones and STK25 KO clones over the indicated time periods. **(C)** Quantification of the percentage of cells remaining in S/G_2 phase following prolonged contact inhibition in hTERT-RPE-1-FUCCI cells transfected with the indicated siRNA. **(D)** Immunoblot and quantification of YAP phosphorylation in IMR90 fibroblasts transfected with the indicated siRNA and held in suspension for the indicated time periods. **(E)** Cytokinesis failure was pharmacologically induced in hTERT-RPE-1 cells to generate binucleated tetraploid cells, and the percentage of EdU positive tetraploid cells following siRNA transfection was quantified. Cells were stained for DNA (White) and EdU incorporation (Green). Scale bar, 20 μm. **(F)** Quantification of the percentage of EdU positive binucleated tetraploid cells following transfection with the indicated siRNA. TP53 siRNA served as positive control. (n=4 biological replicates; *p<0.05, One-way ANOVA with Dunnett's post-hoc test).

A

Cancer Type	Q-value	Frequencies		
		Overall	Focal Deletion	High-Level Deletion
Cervical Squamous Cell Carcinoma	5.99E-43	0.4034	0.2814	0.0068
Sarcoma	2.38E-35	0.4297	0.2734	0.0898
Bladder Urothelial Carcinoma	6.81E-33	0.4297	0.2647	0.0172
HNSCC	2.08E-26	0.4951	0.1935	0.0000
Kidney Cancers	1.05E-25	0.2989	0.0578	0.0023
Brain Lower Grade Glioma	6.16E-24	0.1259	0.1014	0.0039
Lung Cancers	1.82E-22	0.1481	0.1396	0.0000
Lung Squamous Cell Carcinoma	2.71E-21	0.2183	0.2136	0.0000
Kidney RCC Carcinoma	1.93E-19	0.0947	0.0701	0.0019
Glial Cancers	4.42E-17	0.1239	0.0670	0.0018
Breast Invasive Adenocarcinoma	5.75E-16	0.2944	0.1157	0.0019
Ovarian Serous Cystadenocarcinoma	3.19E-15	0.3040	0.2228	0.0121
Stomach Adenocarcinoma	4.89E-6	0.1633	0.1043	0.0000
All Cancers	**5.6E-223**	**0.1892**	**0.1050**	**0.0049**

B

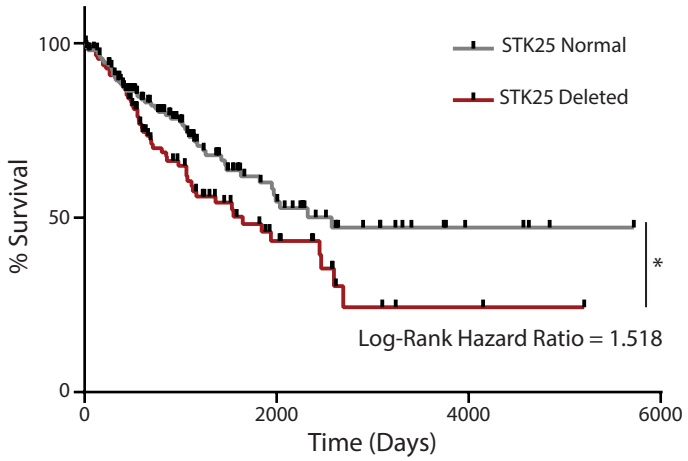

C

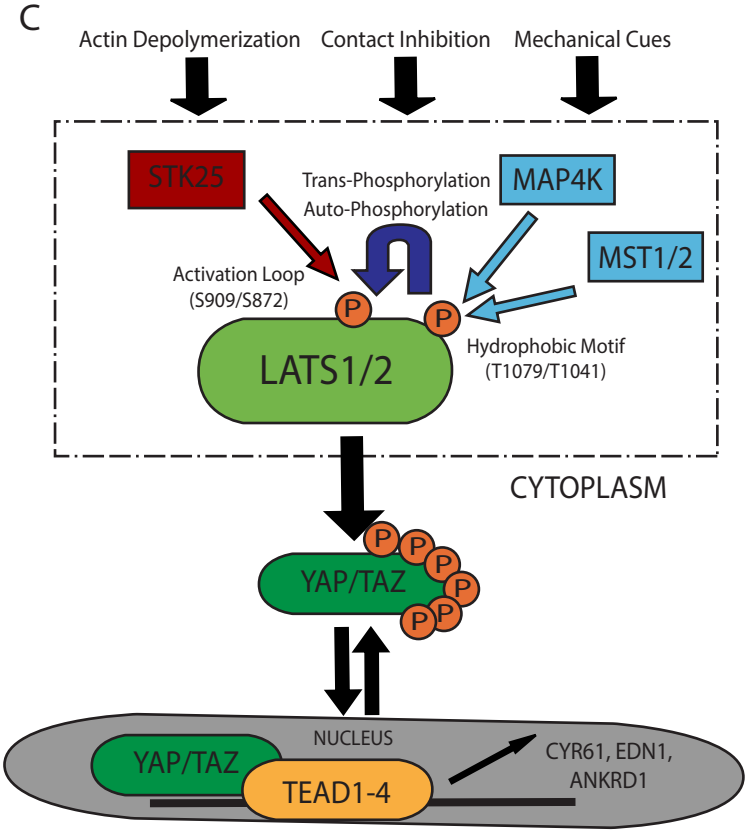

Lim_Fig7

Figure 7. Loss of STK25 is common in human cancers and adversely affects patient survival.

(A) Publicly available TCGA datasets were probed to assess rates of focal deletion in *STK25* using the Tumorscape program online (http://www.broadinstitute.org/tcga/). The top 10 cancers with the highest rates of focal deletions in *STK25* are shown, together with the "All Cancers" dataset. **(B)** Survival data of sarcoma patients from the TCGA dataset were accessed using the Xenabrowser online program (https://xenabrowser.net/) and overall survival rates and times were assessed for patients with and without deletions of *STK25* (*$p<0.0172$, $n=215$, log-rank test). **(C)** Proposed model of STK25 in Hippo tumor suppressor signaling.

SUPPLEMENTAL MATERIALS

Identification of STK25 as a direct activator of LATS signaling

Sanghee Lim[1], Tenny Mudianto[1, 3], Hatim M. Mustaly [1], Ian Paolo Morelos Mauricio [1], Marc A. Vittoria [1], Ryan J. Quinton[1], Brian W. Howell [4], Hauke Cornils[5], Neil J. Ganem [1,2*].

[1]The Laboratory of Cancer Cell Biology, Department of Pharmacology and Experimental Therapeutics, Boston University School of Medicine, Boston, MA.
[2]Division of Hematology and Oncology, Department of Medicine, Boston University School of Medicine, Boston, MA.
[3]Department of Medical Oncology, Dana-Farber Cancer Institute, Harvard Medical School, Boston, MA.
[4]Department of Neuroscience and Physiology, SUNY Upstate Medical University, Syracuse, NY.
[5]Evotec, Hamburg, Germany.

Itemized List of Contents

Supplemental Table S1.

Targets	Sequences	Manufacturer
Non-Targeting #1	UGGUUUACAUGUCGACUAA	Dharmacon GE
STK4 SmartPool	CCAGAGCUAUGGUCAGAUA GCCCUCAUGUAGUCAAAUA GAUGGGCACUGUUCCGAGUA UAAAGAGACCGGCCAGAUU	Dharmacon GE
STK3 SmartPool	GCCCAUAUGUUGUAAAGUA CCACAAGCACGAUGAGUGA GAACUUUGGUCCGAUGAUU CAUGAACCCUUCCCUAUGU	Dharmacon GE
STK24 SmartPool	UAUUAUGGAUCCUAUCUGA UCGAUUAUCUCCAUUCGGA CCAAGAAUCUCGAGAAUGG AGAAAGUGGUUGCCAUAAA	Dharmacon GE
STK25 SmartPool	CUAAAGAGCACCAAGCUAU UCUACAAGGGCAUCGAUAA ACACGCAGAUUAAGAGGAA GCACUGGACUUGCUUAAAC	Dharmacon GE
MAP4K1 SmartPool	GAUACAAAUGAGCUGUGUGA CAACAACGUUCUCAUGUCU GGAGUUAUCUCUUGGUUGCA GAAAGGACCCUCCAUUGGG	Dharmacon GE

MAP4K2 SmartPool	GCGCAAAGGUGGCUACAAU GGACAGGGACACAAUCCUA GGAAUGACCGCUUGUGGAU CGCCCAAACUGAGAGAUAA	Dharmacon GE
MAP4K3 SmartPool	CAAUCGAGCUGUUGGAUAA GAAGUGUUGUGUUGUAAGA UGUUAACACUGGUGAAUUA GGAGCUAACAUUCUAUUAA	Dharmacon GE
MAP4K4 SmartPool	GGGAAGGUCUAUCCUCUUA GACCAACUCUGGCUUGUUA UAAGUUACGUGUCUACUAU UAUAAGGGUCGACAUGUUA	Dharmacon GE
MAP4K5 SmartPool	GGAGAGAGAUACCGUUUUA CGAAUCAGGUAGUUCAGUU GGUCAUCAACAUUCCAUAA GAACAGUUAUUUCCACGGA	Dharmacon GE
MINK1 SmartPool	UGAAAUACGAGCGGAUUAA UCAUGACUCUGAACCGUAA GGAGGACUGUAUCGCCUAU GAACAGCUAUGACAUCUAC	Dharmacon GE
TNIK SmartPool	GAACAUACGGGCAAGUUUA UAAGCGAGCUCAAAGGUUA CGACAUACCCAGACUGAUA	Dharmacon GE

	GACCGAAGCUCUUGGUUAC	
LATS1 SmartPool	GGUGAAGUCUGUCUAGCAA UAGCAUGGAUUUCAGUAAU GGUAGUUCGUCUAUAUUAU GAAUGGUACUGGACAAACU	Dharmacon GE
LATS2 SmartPool	GCACGCAUUUUACGAAUUC ACACUCACCUCGCCCAAUA AAUCAGAUAUUCCUUGUUG GAAGUGAACCGGCAAAUGC	Dharmacon GE
TP53 SmartPool	GAAAUUUGCGUGUGGAGUA GUGCAGCUGUGGGUUGAUU GCAGUCAGAUCCUAGCGUC GGAGAAUAUUUCACCCUUC	Dharmacon GE
STK25 siGENOME	GCGCACUGCUGUUCAGAUA UAAGAACUGUGCUGACUUG GAAGGUGCCCUGUGCUAUG	Dharmacon GE
STK25 Flexitube	CCGGCCGAGTCCACACAGCAA CACCAAGCTATGGATCATCAT CACGGAGCTCATCGACCGCTA AAGGGCATCGATAACCACACA AAGAACTGTGCTGACTTGGAA	Qiagen

Supplemental Table S2.

Targets	Primer Sequences
Mouse genes	
Gapdh Forward	TGTTCCTACCCCCAATGTGT
Gapdh Reverse	GGTCCTCAGTGTAGCCCAAG
Ctgf Forward	GGGCCTCTTCTGCGATTTC
Ctgf Reverse	ATCCAGGCAAGTGCATTGGTA
Cyr61 Forward	TAAGGTCTGCGCTAAACAACTC
Cyr61 Reverse	CAGATCCCTTTCAGAGCGGT
Ankrd1 Forward	AAACGGACGGCACTCCACCG
Ankrd1 Reverse	CGCTGTGCTGAGAAGCTTGTCTCT
Human Genes	
GAPDH Forward	GAGTCAACGGATTTGGTCG
GAPDH Reverse	CATTGATGGCAACAATATCCAC
CTGF Forward	CCAATGACAACGCCTCCTG
CTGF Reverse	TGGTGCAGCCAGAAAGCTC
CYR61 Forward	AGCCTCGCATCCTATACAACC
CYR61 Reverse	TTCTTTCACAAGGCGGCACTC
EDN1 Forward	TGTGTCTACTTCTGCCACCT
EDN1 Reverse	CCCTGAGTTCTTTTCCTGCTT

Supplemental Figure Legends

Supplemental Figure S1. Loss of STK25 decreases YAP phosphorylation in response to actin disruption.

(A) Representative immunoblot of YAP phosphorylation following treatment with 10 μM DCB in IMR90 fibroblasts transfected with the indicated siRNA. **(B)** Quantitation of the IMR90 focused kinome screen (n=3, *p<0.05 by One-Way ANOVA with Dunnett's post-hoc analysis). **(C)** Representative immunoblot of YAP phosphorylation following treatment with 10 μM DCB in hTERT-RPE-1 cells transfected with the siRNA. **(D)** Quantitation of the RPE-1 secondary kinome screen (n=4, *p<0.05, ***p<0.001 by One-Way ANOVA with Dunnett's post-hoc analysis). **(E)** Representative immunoblot of YAP phosphorylation following treatment with 1 μg/mL Latrunculin A in HEK293A cells transfected with the indicated siRNA. **(F)** Immunoblot and **(G)** quantitation of YAP phosphorylation and STK25 protein levels following treatment with 10 μM DCB in HEK293A cells transfected with the indicated siRNA. STK25 protein levels were normalized to GAPDH protein levels and plotted against the respective P-YAP/YAP ratios. Linear regression was performed to assess whether a correlation existed between levels of STK25 protein expression and P-YAP/YAP ratios (p=0.0176, Pearson's $R^2 = 0.5768$).

Supplemental Figure S2. Loss of STK25 increases levels of active, nuclear YAP.

(A) MEFs isolated from STK25+/+, STK25+/-, and STK25-/- mice were plated on coverslips and stained for YAP (Green), Actin (Red), and DNA (White). Scale bar, 20 μm. **(B)** YAP intensity was quantified and nuclear:cytoplasmic ratios were calculated for the MEF images (n>150 per group over 3 biological replicates; **p<0.01, ****p<0.0001 by Kruskal-Wallis test with Dunn's post-

test). **(C)** YAP localization in the MEFs was quantified (n=3 biological replicates, N>C, YAP is enriched in the nucleus; N=C, YAP is evenly distributed between the nucleus and the cytoplasm; N<C, YAP is enriched in the cytoplasm). **(D)** hTERT-RPE-1 transfected with the indicated siRNA were stained for YAP (Green), Tubulin (Red), and DNA (White). Scale bar, 20 μm. **(E)** YAP intensity was quantified and nuclear:cytoplasmic ratios were calculated for the RPE-1 experiments (n=225 over 3 biological replicates; ****p<0.0001 by Mann-Whitney test). **(F)** YAP localization in the hTERT-RPE-1 cells was quantified (n=3 biological replicates, N>C, YAP is enriched in the nucleus; N=C, YAP is evenly distributed between the nucleus and the cytoplasm; N<C, YAP is enriched in the cytoplasm). **(G)** IMR90 fibroblasts transfected with the indicated siRNA were stained for YAP (Green), Actin (Red), and DNA (White). Scale bar, 20 μm. **(H)** YAP intensity was quantified and nuclear:cytoplasmic ratios were calculated (n=300 per group over 4 biological replicates; ****p<0.0001, Mann-Whitney test). **(I)** YAP localization in the IMR90 cells was quantified (n=4 biological replicates, N>C, YAP is enriched in the nucleus; N=C, YAP is evenly distributed between the nucleus and the cytoplasm; N<C, YAP is enriched in the cytoplasm).

Supplemental Figure S3. Cells depleted of STK25 exhibit enrichment of active YAP/TAZ gene signatures.

(A) A list of genes upregulated upon knockdown of STK25 were assessed by GSEA using a list of curated publicly available active YAP/TAZ gene sets. The remainder of the curated list, excluding the top three gene sets already presented, are shown here; with the exception of the Park et al. YAP-TEAD 2017 gene set, which can be found under the accession code GSE32597, and the Quinton YAP-TAZ gene set, which can be found under the accession code GSEXXXXX, the names of the gene sets correspond to the publications from which they were derived. **(B)** A table showing relative enrichment of active YAP/TAZ gene sets in comparison to enrichment of

Hallmark gene sets from the Molecular Signatures Database is presented.

Supplemental Figure S4. STK25 acts independent of the canonical MST/MAP4K axis to regulate YAP.

(A) Immunoblot and quantitation of YAP phosphorylation following transfection with the indicated siRNA in MM8KO cells grown to confluence to activate Hippo signaling (n=3, *p<0.05 by unpaired t-test). **(B)** MM8KO cells were transfected with a vector encoding FLAG-tagged wild-type STK25, and were stained for YAP (Green), FLAG (Red), and DNA (White). Scale bar, 20 μm. Arrows indicate examples of FLAG signal-positive cells. **(C)** YAP intensities were quantified in a FLAG-signal positive cell as well as a FLAG-signal negative cell immediately adjacent to it, and nuclear:cytoplasmic ratios were calculated (n=100 per group over 3 biological replicates; ****p<0.0001, Mann-Whitney test).

Supplemental Figure S5. STK25 activates the LATS kinases.

(A) IP purified wild-type LATS2 (HA-LATS2-WT) from transfected MM8KO 293A cells was co-incubated with IP purified FLAG-STK25-WT, FLAG-STK25-KD, or FLAG-MAP4K1, all from transfected MM8KO 293A. Kinase reactions were allowed to occur in the presence of 500 μM ATP, and levels of phosphorylated LATS at the hydrophobic motif (P-LATS-HM) and activation loop motif (P-LATS-AL) were assessed via immunoblotting. A mock IP product from untransfected MM8KO 293A lysates using FLAG antibody and protein G magnetic beads served as control. **(B)** LATS dKO 293A were transfected with empty vector, wild-type LATS2 (HA-LATS2-WT), or kinase-dead LATS2 (HA-LATS2-KD), alongside Vector, wild-type STK25 (FLAG-STK25-WT), or kinase-dead STK25 (FLAG-STK25-KD). Lysates were collected and

assessed via SDS-PAGE and immunoblotting for YAP phosphorylation at serine127. Quantitation of YAP phosphorylation under the various transfection conditions are presented (n=3, ***p<0.001, One-Way ANOVA with Tukey's post-hoc test).

Supplemental Figure S6. STK25 loss impairs physiologic Hippo activation.

(A) Representative phase images of HEK293A grown to low or high confluence following transfection with the indicated siRNA. Scale bar, 100 μm. **(B)** Global phosphorylation status of YAP was assessed via phos-tag gel electrophoresis using lysates from HEK293A grown to either low or high confluence following transfection with the indicated siRNA. **(C)** Global phosphorylation status of TAZ was assessed via phos-tag gel electrophoresis using lysates from HEK293A grown to either low or high confluence following transfection with the indicated siRNA. **(D)** Immunoblot and quantitation of phosphorylated YAP levels under conditions of high confluence in either control HEK293A stably expressing Cas9 and a non-targeting sgRNA or STK25 KO 293A stably expressing Cas9 together with either sgRNA 1 (Clone 1) or sgRNA 2 (Clone 2) targeting STK25. (n=4; **p<0.01, One-way ANOVA with Dunnett's post-hoc analysis).

Supplemental Figure S7. Focal deletions of identified Hippo pathway components are rare.

(A) Rates of recurrence-free survival in sarcoma patients with and without deletions in *STK25* (n=125 for patients without deletions, n=90 for patients with deletions, *p<0.05, two-tailed chi-square goodness-of-fit test). **(B)** Publicly available TCGA datasets were probed to assess rates of focal deletion in known upstream activators of LATS kinases, using the "All Cancers" dataset from the Tumorscape program online (http://www.broadinstitute.org/tcga/).

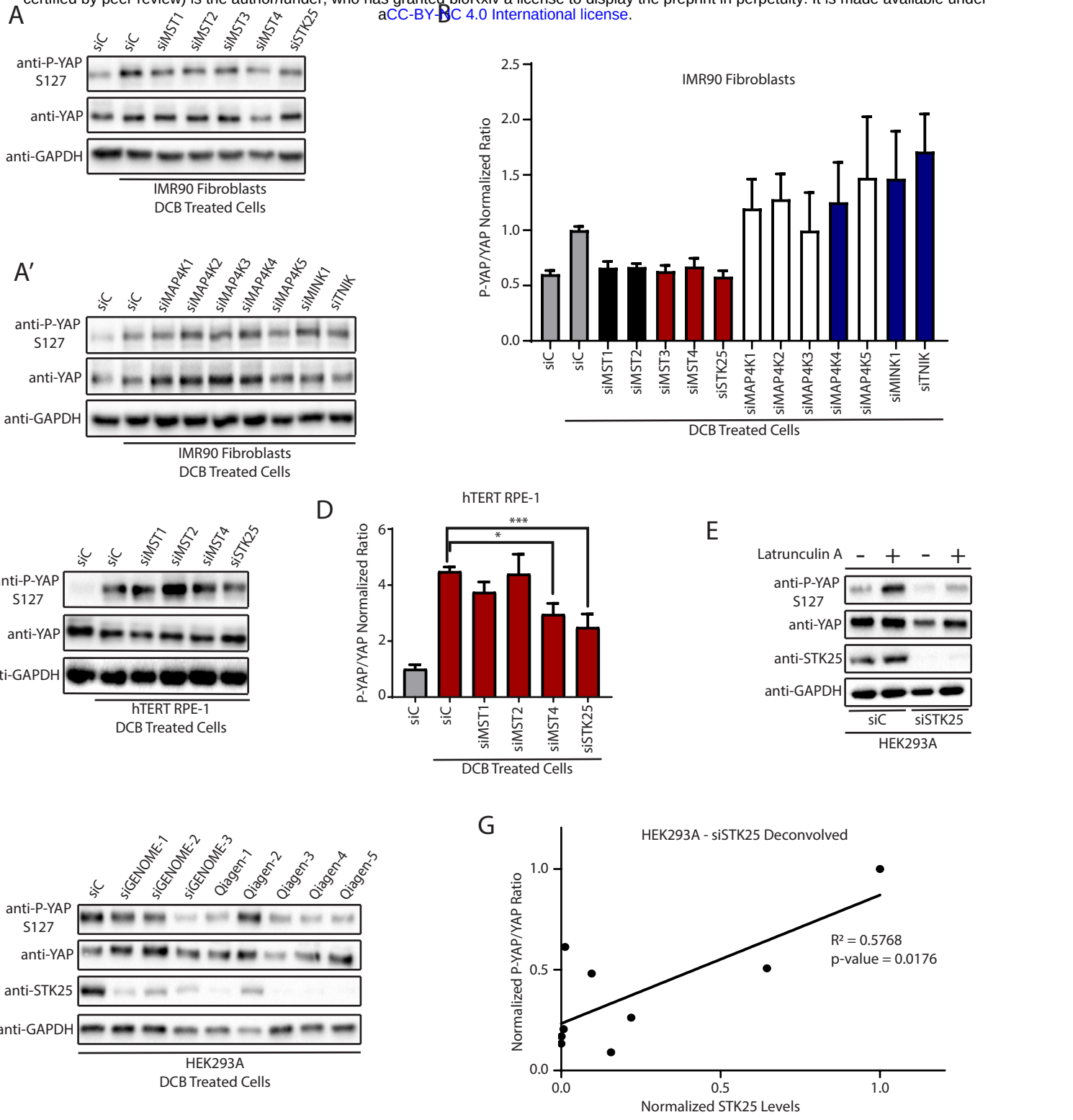

Lim_Supplemental_Figure_S1

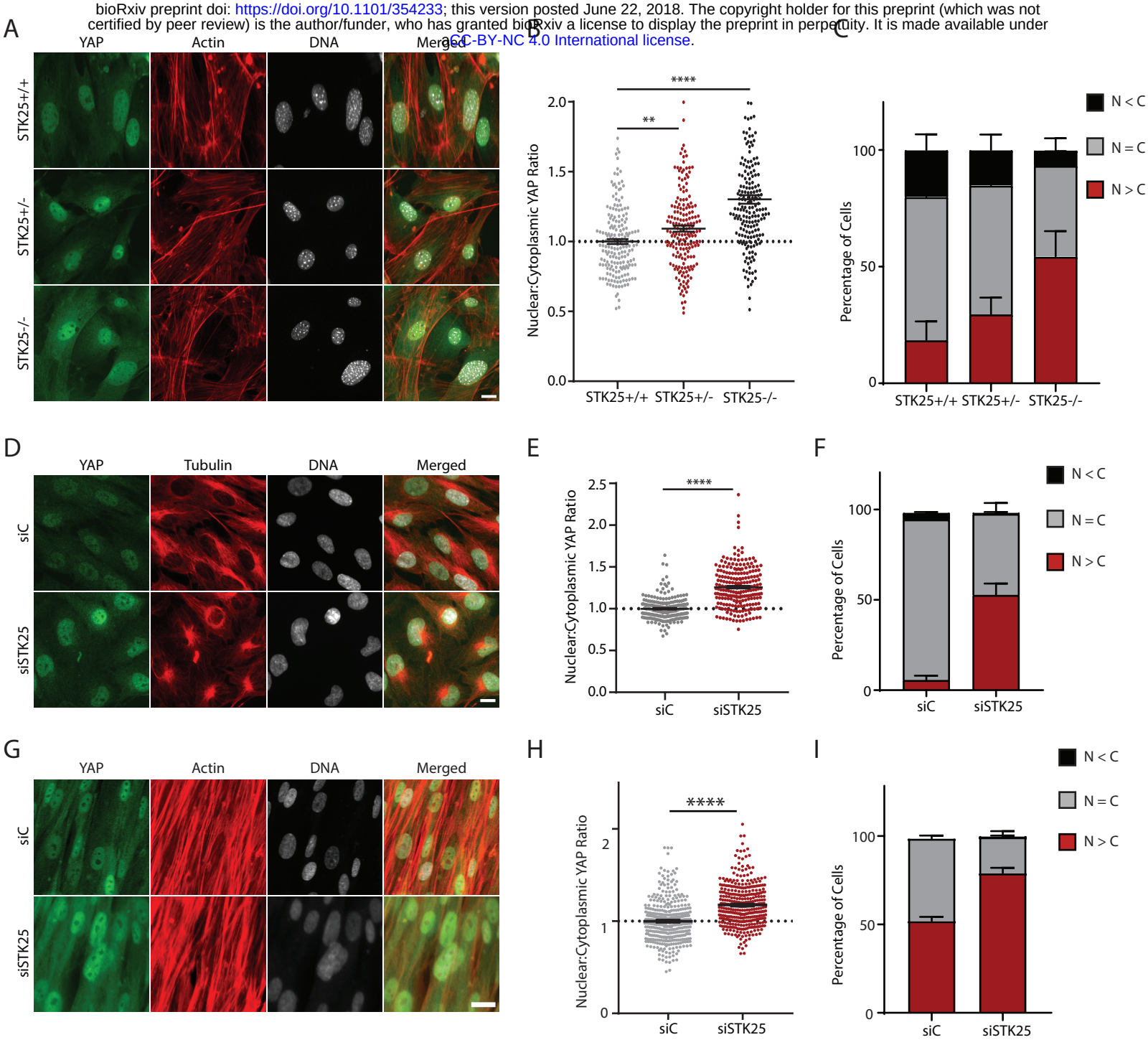

Lim_Supplemental_Figure_S2

A

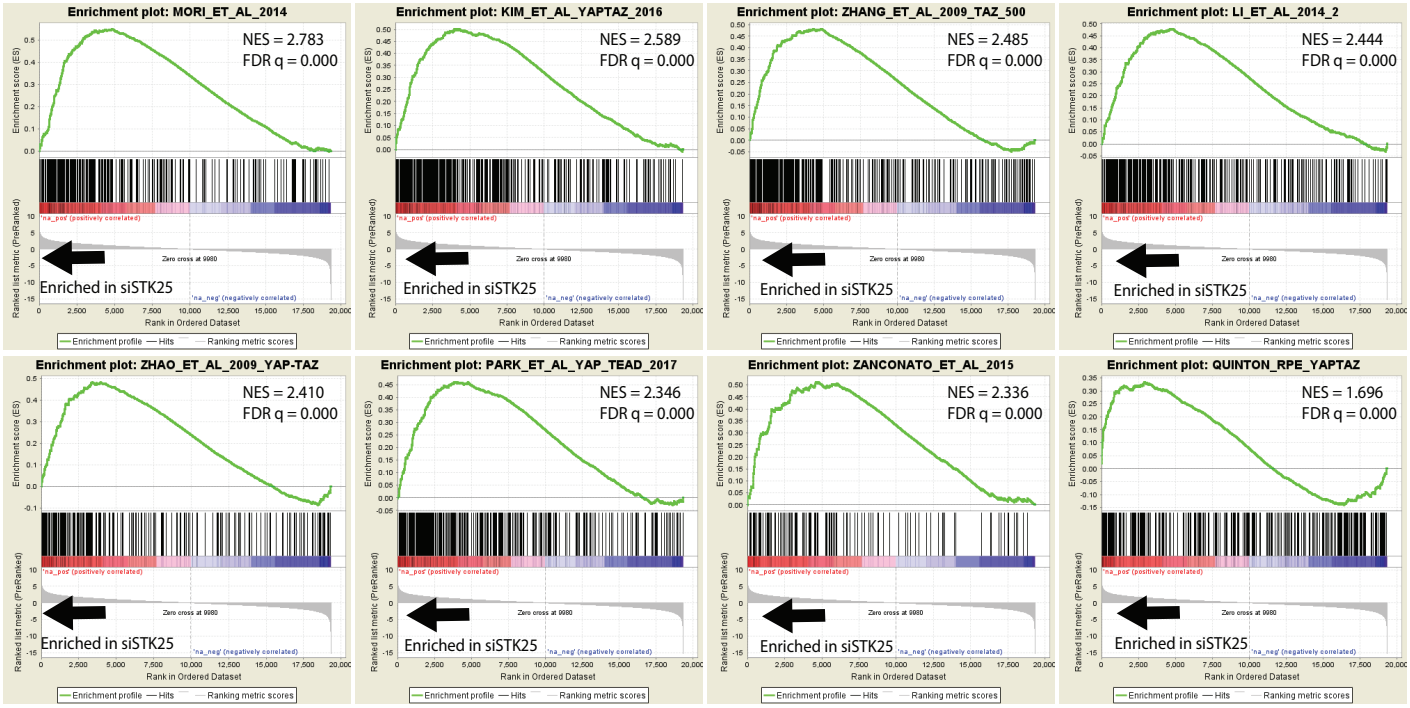

B

Annotated Cellular Function/ Published YAP/TAZ gene set	Enrichment Score	Normalized Enrichment Score	FDR q-value
Park et al. 2016	**0.62**	**3.17**	**0.000**
HALLMARK_MYC_TARGETS_V1	*0.64*	*3.06*	*0.000*
HALLMARK_E2F_TARGETS	*0.63*	*3.04*	*0.000*
Enzo et al. 2015	**0.59**	**3.01**	**0.000**
Mohseni et al. 2014	**0.55**	**2.84**	**0.000**
Mori et al. 2014	**0.55**	**2.77**	**0.000**
HALLMARK_OXIDATIVE_PHOSPHORYLATION	*0.56*	*2.66*	*0.000*
Kim et al. 2016 – YAP/TAZ	**0.50**	**2.60**	**0.000**
Zhang et al. 2009 - TAZ	**0.48**	**2.50**	**0.000**
HALLMARK_G2M_CHECKPOINT	*0.51*	*2.46*	*0.000*

Lim_Supplemental_Figure_S3

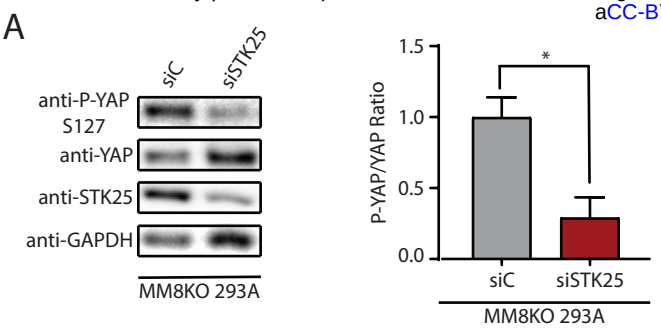

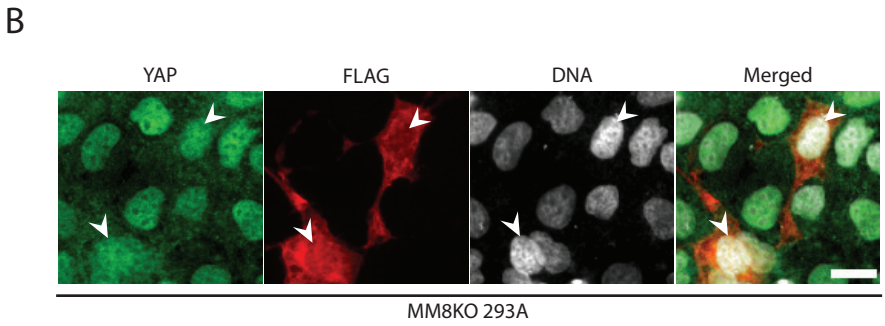

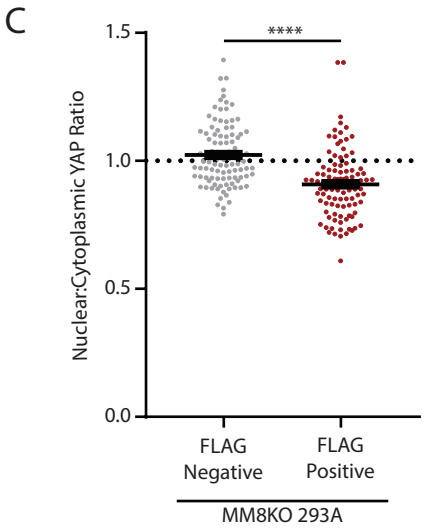

Lim_Supplemental_Figure_S4

A

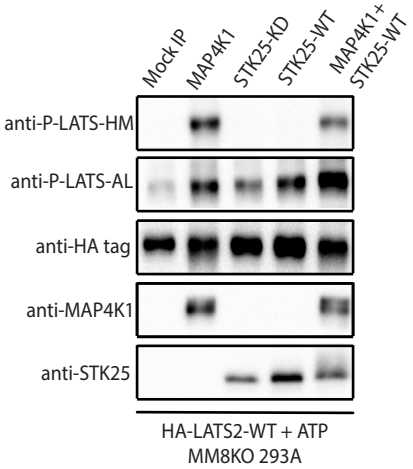

B

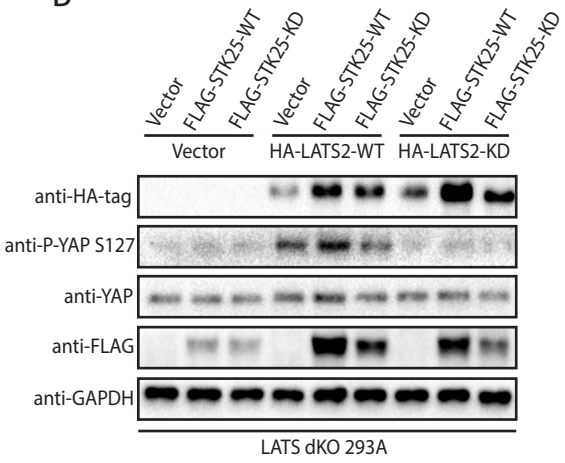

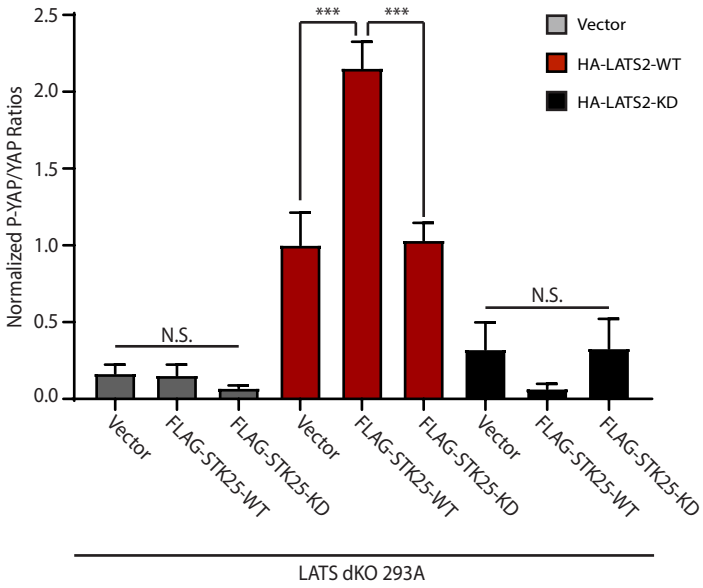

Lim_Supplemental_Figure_S5

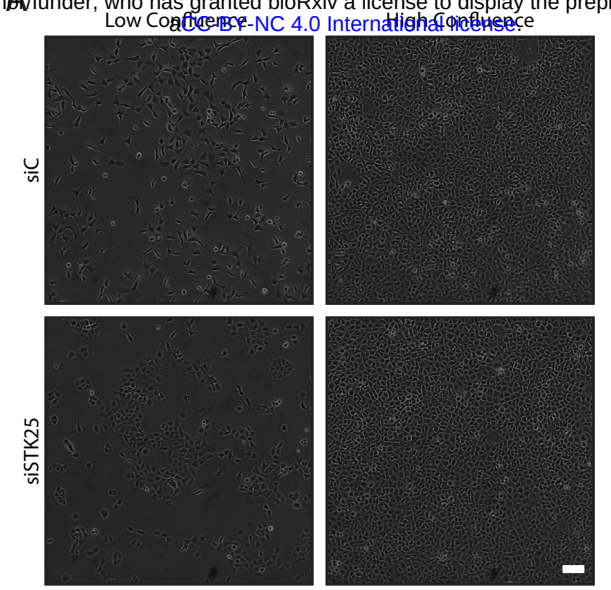

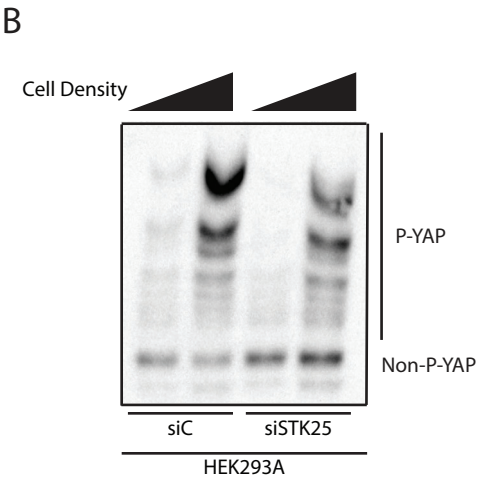

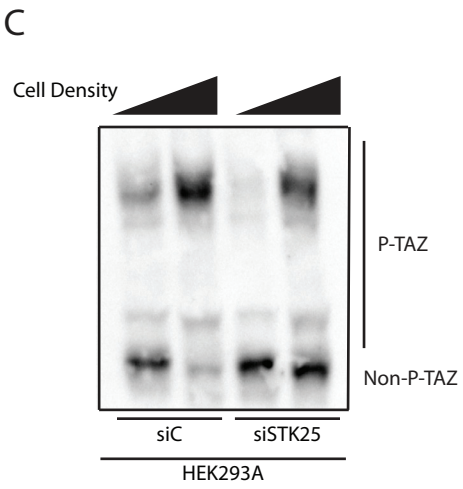

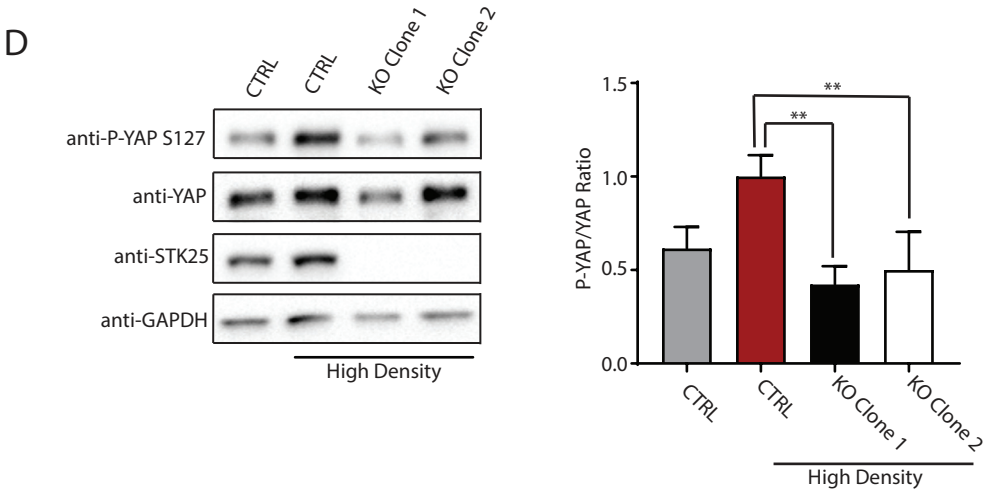

Lim_Supplemental_Figure_S6

A

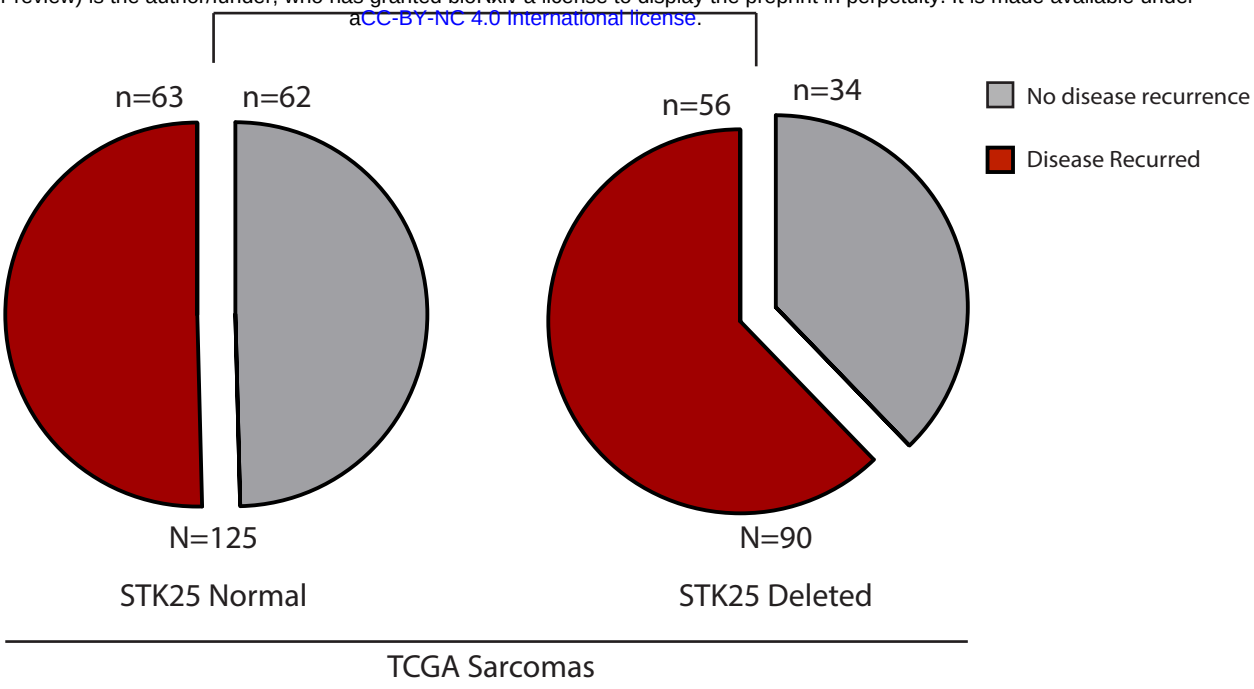

B

Gene	Amplified/Deleted	Q-value	Overall Frequency
MST1	Neither	N/A	N/A
MST2	**Amplified**	**1.07 E-15**	**0.4231**
MAP4K1	**Amplified**	**1.36 E-37**	**0.2158**
MAP4K2	Neither	N/A	N/A
MAP4K3	Neither	N/A	N/A
MAP4K4	Neither	N/A	N/A
MAP4K5	Neither	N/A	N/A
TNIK/MAP4K6	**Amplified**	**7.75 E-217**	**0.3284**
MINK1/MAP4K7	Neither	N/A	N/A
TAOK1	**Amplified**	**1.55 E-7**	**0.1857**
TAOK2	Neither	N/A	N/A
TAOK3	Neither	N/A	N/A
STK25	**Deleted**	**5.61 E-223**	**0.1892**

Lim_Supplemental_Figure_S7